N84-27319

NASA

Technical Memorandum 83916

MATRIX PARTITIONING AND EOF/PRINCIPAL COMPONENT ANALYSIS OF ANTARCTIC SEA ICE BRIGHTNESS TEMPERATURES

C. W. MURRAY, JR., J. L. MUELLER*,
AND H. J. ZWALLY

APRIL 1984

National Aeronautics and
Space Administration

Goddard Space Flight Center
Greenbelt, Maryland 20771

*** Oceanographic Department**
Naval Post Graduate School
Monterey, California 93943

TM 83916

MATRIX PARTITIONING AND EOF/PRINCIPAL COMPONENT ANALYSIS OF ANTARCTIC SEA ICE BRIGHTNESS TEMPERATURES

C. W. MURRAY, JR., J. L. MUELLER*, AND H. J. ZWALLY

APRIL 1984

GODDARD SPACE FLIGHT CENTER
Greenbelt, Maryland 20771

* OCEANOGRAPHIC DEPARTMENT
Naval Post Graduate School
Monterey, California 93943

ABSTRACT

A matrix partitioning scheme is presented for approximating EOF's (empirical orthogonal functions) or eigenvectors of a large sample covariance matrix. The data array, a field of measured anomalies of some physical variable relative to their time averages, is partitioned in either the space domain or the time domain. Eigenvectors and corresponding principal components of the smaller dimensioned covariance matrices associated with the partitioned data sets are calculated independently, then joined to approximate the eigenstructure of the larger covariance matrix associated with the unpartitioned data set. The accuracy of the approximation $\propto$ (fraction of the total variance in the field) and the magnitudes of the largest eigenvalues from the partitioned covariance matrices together determine the number of local EOF's and principal components to be joined at any particular level.

The accuracy and efficiency of the method are demonstrated by applying the technique to the space-time distribution of Nimbus-5 ESMR (Electrically Scanning Microwave Radiometer) sea ice brightness temperature measurements for a large area of the Antarctic (Weddell Sea) and for the time period extending from 30 September 1973 through 25 May 1975.

From analysis of the spatial EOF's and their coefficients (principal components) maximum and minimum ice extents and the times of these extents can be identified. Regions and periods of ice growth and decay are identified as well as regions and periods of higher changes in growth and decay. The interannual variability in the Weddell Polynya between 1973 and 1974 is exhibited by the fourth EOF and its principal component. Power spectral analysis of the principal components reveal periods which can be related to the seasonal cycle of sea ice growth and decay in the Weddell Sea, harmonics of this cycle, the cold season (205 days), the warm season (160 days), and the duration of spring-summer ice removal (120 days) as reported in the literature. The first four EOF's and their components can be considered the dominant normal modes of variation in the ice field, accounting for 85% of the total information content in the data (field variance).

1.0 INTRODUCTION

Empirical orthogonal function (EOF) analysis, or the method of principal components (also singular value decomposition) is well-documented in the literature and has found wide application in many areas of applied research, particularly in those areas where there are large numbers of measurements. For large data sets (or geophysical fields) it becomes increasingly important to find ways of compressing the data while still extracting as much of the information content as possible.

EOF's, which are linear functions of the measurements, provide us with an efficient tool in data compression and information extraction. The method is efficient in the sense that highly correlated fields can be adequately represented by the least number of orthogonal functions and corresponding orthogonal coefficients (principal components). The higher the correlation in the measurements, the fewer the number of functions and coefficients are required to describe the data and explain the variance in the field. This reduces the dimensionality of the problem. The latter feature is especially important in the development of statistical prediction schemes that rely upon multiple linear regression techniques, since the skill and confidence of these schemes depend to a large extent upon á priori methods of reducing the number of available predictors (Davis, 1976; Barnett and Hasselmann, 1979).

A property of EOF's which makes them particularly appealing is that, unlike conventional orthogonal representations (e.g., the familiar Fourier decomposition, Tschebycheff polynomials, or spherical harmonics), they do not require any predetermined form. Rather, since they are derived as the eigenvectors of the covariance matrix between the variables (which can be computed for any variable observed on any grid, regular or not), their form depends directly on the interrelationships existing within the data itself. This feature is especially desirable when analyzing fields such as sea surface temperature, pressure, or sea ice brightness temperature anomalies, which have no known analytic form and depend on complex boundary conditions. Also, the derived eigenvectors often provide us with a tool for gaining insight into the physical

interpretation of underlying complex processes within a geophysical field.

The first EOF is that linear combination of the original variables, which when used as a linear predictor of these variables, explains the largest fraction of the total variance. The second, third EOF, etc., explain the largest parts of the remaining variance. The ordered set of EOF's and their coefficients are frequently referred to as the normal (also natural, principal) modes of variation in the field. The lower ordered EOF's not only account for the largest fraction of the total variance, but their coefficients often show large scale frequency variations. The higher ordered EOF's usually show small spatial scales with their coefficients being characterized by diminished amplitudes and higher frequencies, both of which are sometimes associated with noise.

Early references on principal components can be found in Pearson (1901) and Frisch (1929) who were concerned with fitting a line, a plane, or in general a subspace to a scatter of points in a higher dimensional space. Principal components as applied to random variables were introduced by Hotelling (1933) who characterized them by certain optimal properties. Since then, they have been characterized by slightly different properties (Girschick 1936, Anderson 1958, Kullbach 1959, Anderson 1963, Darroch 1965, Okamoto 1968). A good treatment of the subject can be found in Kendall (1957), Kshirsagar (1972), Marriott (1974), and Kendall (1975). An excellent paper on the use and interpretation of principal components in applied research can be found in Rao (1964). This reference contains proofs of a number of optimal properties of principal components. One of the more important properties states that the eigenvectors of the sample covariance matrix comprise an optimal set of basis functions for a given truncation k. That is, for a given truncation k, no other basis set can explain more of the average variance (Davis 1976, Appendix A).

Fukuoka (1951) used principal components in a study of 10-day forecasts and Lorenz (1956) was the first investigator to use the term "empirical orthogonal functions" (eigenvectors of a sample covariance

matrix, also characteristic vectors) in connection with statistical weather forecasting. Gilman (1957) subsequently applied EOF's to 30-day forecasts using data from 40 winters to calculate eigenvectors of temperature over the United States, and pressure over the Northern Hemisphere. Sellers (1968) computed eigenvectors for precipitation over the western United States for each month of the year and Kutzbach (1970) calculated eigenvectors for the January and July sea level pressure fields over the Northern Hemisphere. Kidson (1975) derived EOF's for temperature, precipitation, and sea level pressure in both the Northern and Southern Hemisphere and in the tropics using 10 years of data. More recently Barnett (1978) studied winter-averaged and annually-averaged surface temperature eigenvectors over Northern Hemisphere land and ocean areas for the 1950 - 1977 time period. Trenberth (1975) and Davis (1978) used EOF's to study air-sea interactions and Walsh and Johnson (1979) analyzed associations between interannual atmospheric variability and arctic sea ice extent.

Excellent references for the derivation of EOF's and their coefficients as well as procedures for calculating them can be found in Kutzbach (1967), Sellers (1968), and Davis (1976). Hotelling (1933), Bartlett (1954), Lawley (1956), Buell (1978), Preisendorfer and Barnett (1977, 1978) discuss significance tests for EOF's, and Craddock and Flood (1969), Craddock and Flintoff (1970), and Rinne and Järvenoja (1979) outline procedures for truncating the EOF series.

Buell (1972) has a very interesting discussion on the integral representation of the eigenvalue problem and compares it with the matrix formulation. He states "...the integral representation is appropriate for meteorological problems since additional considerations based on the properties of a continuum are possible, necessary, and desirable." In two or more dimensions the shape of the boundary that defines the area of integration must be taken into account. If the area of each grid is the same, the two formulations are equivalent. This is essentially true for the data set discussed in the present paper. The shape of the boundary is also pursued in Buell (1975, 1979).

Craddock (1973) discusses the reduction of the dimensionality of the problem of long range weather forecasting and mentions significant advances in the application of eigenvector techniques in meteorology.

North, Bell, and Cahalan (1982) give an excellent review of EOF's, focusing attention on the necessary weighting factors for gridded data and the sampling errors incurred when too small a sample is available. A rule of thumb is presented for indicating when an EOF is likely to be subject to large sampling errors.

The number of applications of EOF analysis and the list of parameters which have been expanded in terms of EOF's is quite extensive. Atmospheric parameters which have been expanded include pressure (geopotential), temperature, humidity, water-vapor mixing ratio, rainfall, wind velocity components, and ozone content (Obukhov 1960, Rukhovets 1963, Holmstrom 1963, Grimmer 1963, Garrilin 1965, Popov 1965, Koprova and Malkevich 1965, Mateer 1965, Marchuk 1965, Wark and Fleming 1966, Alishouse et. al 1967, Kutzbach 1967, Sellers 1968, Yakovleva et. al 1968, Sellers and Yarger 1969, Craddock and Flood 1969, Craddock and Flintoff 1970, Bodin 1974, Kidson 1975, Weare 1976, 1979, 1982). Spurrell (1963) has applied EOF's to metallurgical data, Choi (1967) to the analysis of seismic data, Smith et. al (1972, 1976) to retrieve atmospheric parameters from spectral radiance measurements, and Mueller (1976) has used EOF/principal component analysis for ocean color spectra. Jalickee and Klepczynski (1977) applied singular value decomposition (principal component analysis) in the compaction of navigation tables (see also Good 1969 and Golub and Reinsch 1970 in connection with singular value decomposition). Steyaert et. al (1978) have used EOF's of sea level pressure as predictors of wheat yields in North America and the Soviet Union. Barnett and Preisendorfer (1978) have formulated eigenvectors of several variables in "key regions", identified through a filtering process, in order to analyze climatic predictability. And, Walsh and Johnson (1979) have studied Arctic sea ice data from the 1953-1977 period, and used EOF's to identify the major spatial and temporal scales of ice fluctuations within the 25-year period.

Yakovleva et. al (1968) present a joining method for combining spatial EOF's and their corresponding time coefficients from two distinct spatial regions in order to approximate the "global" EOF

structure for the larger domain. This technique is applied in Rinne and Karhila (1979) and in this paper.

The purpose of this paper is two-fold: (1) to present a matrix partitioning scheme for approximating EOF's associated with large sample covariance matrices at a fixed tolerance level (or fixed percentage of the total sample variance), and; (2) to apply the method to the EOF/principal component analysis of the Nimbus-5 ESMR (Electrically Scanning Microwave Radiometer) brightness temperature measurements (1.55 cm) of Antarctic sea ice for a large area of the south pole (Weddell Sea region) and for the time period from 30 September 1973 through 25 May 1975. In addition, a physical interpretation of the first four spatial EOF's and their corresponding time coefficients or principal components (which can be considered the dominant normal modes of variation within the ice field) will be given.

Section 2.0 is devoted to a brief description of the relevant mathematical theory associated with the EOF/principal component decomposition. In Section 2.1 the concept of matrix partitioning (in either the spatial domain or the time domain) is introduced. In Section 3.0, previous analyses of ESMR data are cited. The relationships between brightness temperature, emissivity, and sea ice concentration are shown and discussed in Section 3.1. Section 4 contains a description of the particular data set analyzed, the ESMR instrument (spatial and temporal resolution), and the results of an EOF decomposition of the field and application of the partitioning method to the data set. The conclusions are found in Section 5.

2.0 MATHEMATICAL THEORY

In the following V is a real (p x q) data matrix representing the scalar field of measured anomalies of some physical variable relative to their time averages (row means removed). The number of spatial points is p and the number of time points is q. V has rank $r \leq q \leq p$.

The complete singular value decomposition of V (Good 1969, Golub and Reinsch 1970) or the expansion of V in terms of empirical orthogonal functions (EOF's) and their associated coefficients (principal components) is given by (1)

$$\begin{aligned} V &= ED^{\frac{1}{2}}F' = e_1 d_1^{\frac{1}{2}} f_1' + \ldots + e_q d_q^{\frac{1}{2}} f_q' \\ &= EY = e_1 y_1 + \ldots + e_q y_q \\ &= Z'F' = z_1' f_1' + \ldots + z_q' f_q' \\ &= (v_1, \ldots, v_j, \ldots, v_q) = (v_{ij}) \end{aligned} \qquad (1)$$

where the orthonormal vectors e_j (columns of E) are the left singular vectors of V or spatial EOF's (eigenvectors of VV' or of the sample covariance matrix $\hat{S} = VV'/(q-1)$), the orthonormal vectors f_j (columns of F) are the right singular vectors of V or time EOF's (eigenvectors of V'V), the orthogonal vectors y_j (row vectors of Y normalized to d_j) are the principal components in the spatial domain corresponding to the e_j vectors (functions of time), the orthogonal vectors z_j (row vectors of Z also normalized to d_j) are the principal components in the time domain corresponding to the f_j vectors (functions of space), and the $d_j^{\frac{1}{2}}$ are the singular values of V or the non-negative square roots of the eigenvalues of VV' (or of V'V) with

$$d_1^{\frac{1}{2}} \geq d_2^{\frac{1}{2}} \geq \ldots \geq d_q^{\frac{1}{2}} \geq 0$$

---

(1) x' is the transpose of x.

$$D^{\frac{1}{2}} = \text{diag}(d_1^{\frac{1}{2}} \ldots d_q^{\frac{1}{2}})$$

$$E'E = F'F = FF' = I_q \tag{2}$$

$$YY' = ZZ' = D = \text{diag}(d_1 \ldots d_q)$$

Since the rank of V is r [2], $d_{r+1}^{\frac{1}{2}} = \ldots = d_q^{\frac{1}{2}} = 0$.

Using (1) and the orthonormal property of the e_j and f_j vectors in (2) the principal components in the space domain and time domain are, respectively,

$$y_j = d_j^{\frac{1}{2}} f_j' = e_j' V$$

and (3)

$$z_j = d_j^{\frac{1}{2}} e_j' = f_j' V'$$

From (2) and (3), $y_i y_j' = z_i z_j' = d_j \delta_{ij}$, and we see that the principal components are orthogonal functions of the data V, ordered in such a way that the first component y_1 or z_1 (or equivalently e_1 or f_1) corresponding to d_1 accounts for the largest fraction of the trace T_r of VV' (or of V'V), the second component y_2 accounts for the second largest fraction of the trace, and the jth component accounts for

$$(d_j/T_r) \times 100\%$$

of the trace T_r where

$$T_r = d_1 + \ldots + d_q \tag{4}$$

From (1) the jth measurement vector v_j is given by

---

[2] The rank of V, V', VV', and V'V is the same (Noble 1969).

$$v_j = \sum_{k=1}^{q} y_{kj} e_k \qquad (5)$$

where the coefficient y_{kj} associated with the kth eigenvector e_k for the jth time point is the jth element of y_k and represents the amplitude at time j of the normalized (unit length) spatial EOF pattern e_k.

The sum of squares of the coefficient associated with the kth eigenvector, $\sum_{j=1}^{q} y_{kj}^2 = d_k$ is equal to (q-1) times the total variance explained by the kth eigenvector or EOF. The total variance in the field is $T_r/(q-1)$.

From (1) we can also write the scalar representation of the field as

$$v_{ij} = \sum_{k=1}^{q} y_{kj} e_{ik} \qquad (6)$$

which shows that the contribution to the field by the kth spatial EOF at the ith spatial point and jth time point is given by the product of the ith element of e_k and the jth element of the associated time coefficient or principal component y_k.

Since the elements of $y_k = (e_k'v_1, \ldots, e_k'v_q)$ from (3) are the projections of the measured anomaly vectors v_j (j = 1,2,...,q) onto e_k (see Appendix A for a geometrical interpretation of principal components), the y_k are time-dependent amplitude functions which modulate the spatial EOF patterns e_k and describe the temporal variation of the field about the mean in the direction of e_k. For fixed k the e_k, being functions of space only, describe the spatial variation of the field about the mean in this direction, i.e., the spatial distribution of covariance in the field. The ordered spatial EOF's and their associated time coefficients (or principal components) are sometimes referred to as the normal (also natural or principal) modes of variation in the field.

From (1) and (2), V'V = Y'Y, from which we obtain

$$\sum_{n=1}^{p} v_{nj}^2 = \sum_{k=1}^{q} y_{kj}^2 \qquad (7)$$

and therefore

$$(y_{kj}^2 / v_j' v_j) \times 100 \qquad (8)$$

represents the fraction in percent of the total sum of squares of the jth measured anomaly vector (v_j) accounted for by the kth EOF e_k (see Sellers 1968) or equivalently the percent contribution of the kth principal component y_k to the spatially averaged mean square anomaly at the jth time point, $v_j' v_j$.

In Appendix B it is shown that for fixed $k \leq r$, $(V-\bar{V})$ has minimum norm, where $\bar{V}$ is the approximation to V using the first k terms in (1). Thus, the expansion of V in (1) is optimum in the sense of least squares. Each successive term in the expansion more closely approximates V with the complete reconstruction of the data being accomplished when k = r. For highly correlated data arrays or fields the first few EOF's will account for the largest fraction of the total information content in the data (trace T_r of VV'). Therefore, representing the field using these few terms leads to a reduction in the dimensionality of the problem. It is in this sense that the singular value decomposition or EOF/principal component expansion of V provides us with the most efficient method for data compression (see Jalickee and Klepczynski 1977).

It is shown in Appendix B that VV' and V'V have the same nonzero eigenvalues and that if e_j is an orthonormal eigenvector of VV' corresponding to $d_j \neq 0$ with principal component y_j, then $f_j = d_j^{-\frac{1}{2}} y_j'$ is an orthonormal eigenvector of V'V also corresponding to $d_j \neq 0$. Also, if f_j is an orthonormal eigenvector of V'V corresponding to $d_j \neq 0$ with principal component z_j, then $e_j = d_j^{-\frac{1}{2}} z_j'$ is an orthonormal eigenvector of VV' corresponding to d_j. The duality between the principal components and eigenvectors in the two domains is evident from the relations in (3). This result can afford us savings in both computer storage requirements and computation time in the calculation of eigenvalues and eigenvectors, especially if one of the dimensions of V is much larger than the

other. The eigenstructure of the smaller dimensioned matrix (either VV' or V'V) can be calculated first. Then, from this structure the eigenvectors of the larger dimensioned matrix can be easily obtained.

If both dimensions of V are large, V can be partitioned into a number of smaller subarrays V_i and the eigenstructure of the smaller dimensioned matrices - either $V_i V_i'$ or $V_i' V_i$ - calculated. Then, by properly joining eigenvectors and principal components from each partition, the eigenstructure of VV' (or of V'V) can be obtained to any required accuracy α ($0 \leq \alpha \leq 1$) where α represents a fraction of the trace T_r. The number of vectors and components to be joined at any particular level is a function of α, T_r, and the magnitudes of the largest eigenvalues of $V_i V_i'$. The method for joining vectors from various subdivisions of the data has been presented before by Yakovleva et. al (1968) and also by Rinne and Karhila (1979). In application of the joining procedure these authors have partitioned the data in the spatial domain, joining together a fixed number of spatial EOF's from each partition. In the present analysis V is partitioned in both the space and time domains and only that number of vectors (and components) are joined at each level which are sufficient to insure that $100\alpha\%$ of the trace T_r is accounted for.

2.1 MATRIX PARTITIONING AND JOINING VECTORS

Partitioning of the basic data array V into a number of subarrays with the subsequent joining of local EOF's from these subdivisions offers two advantages. First, the procedure provides us with an efficient algorithm for approximating the eigenstructure of VV' (or of V'V) at a specified tolerance level α. Second, joining local EOF's from these particular subdivisions enables us to gain an insight into the global EOF structure through analysis of the joining vectors. The joining vectors (eigenvectors of the covariance matrix of principal components from the various subdivisions) are essentially weighting functions with the elements of each vector weighting specific local EOF's to the global EOF associated with that particular vector. Since the elements range in value from -1 to +1 joining vectors can also be viewed as correlation functions. In this sense each element gives us a measure of the correlation between the local EOF and the global EOF. These interpretations of the joining vectors are useful in interpreting global EOF's.

Sets of EOF's associated with the various subdivisions of the data may be joined together in a number of ways. The procedure for joining M sets in one operation is an extension of the procedure for joining two sets in one operation (this latter procedure is described in Yakovleva et. al 1968 and in Rinne and Karhila 1979) and is shown in Appendix C. Appendix D contains a general procedure for joining where there are L partition levels, M_l matrices and N_l groups of matrices at the lth level ($l = 1,2,\ldots,L$).

For purposes of this discussion we will consider partitioning in the spatial domain only. To apply the procedure of joining in the time domain the transpose of V, or V', can be used. The algebraic equations and manipulations which apply for V will then apply for V'. Thus, let us partition V in (1) into M submatrices V_i each of dimension (p_i x q) and rank $r_i \leq \min(p_i,q)$ with $p_1 + \ldots + p_M = p$ and $r_1 + \ldots + r_M \geq r$.

$$V = \begin{pmatrix} V_1 \\ \vdots \\ V_M \end{pmatrix} \tag{9}$$

From Appendix C, V can be written as

$$V = \overline{EY} = \overline{E}(A\overline{D^2}H')$$

$$= GW = g_1 w_1 + \ldots + g_r w_r \tag{10}$$

where

$$\overline{E} = \begin{pmatrix} E_1 & & \\ & \ddots & \\ & & E_M \end{pmatrix}$$

$$\overline{Y} = \begin{pmatrix} Y_1 \\ \vdots \\ Y_M \end{pmatrix}$$

The columns of E_i in $\overline{E}$ are the local spatial EOF's for the ith subdivision V_i and the rows of Y_i in $\overline{Y}$ are the corresponding principal components. Since the rows of $\overline{Y}$ are correlated, $\overline{Y}$ is expressed in terms of its singular value decomposition $A\overline{D^2}H'$. From (10) and using (1), since E_i is $(p_i \times r_i)$ and Y_i is $(r_i \times q)$ we have $E = G = \overline{E}A$ and $Y = W = \overline{D^2}H'$. The joining vectors are the columns of A which are the eigenvectors of $\overline{YY}'$. The columns of E (or equivalently G) are the spatial global EOF's and the rows of Y (or equivalently W) are the corresponding time coefficients or principal components.

It is also shown in Appendix C that if $k_i \leq r_i$ $(i=1,2,\ldots,M)$ and $\bar{k} \leq k_1 + \ldots + k_M$ are the smallest integers such that

$$\sum_{j=1}^{k_i} {}_i d_j \geq \alpha T_i \qquad (11)$$

and

$$\sum_{j=1}^{\bar{k}} \bar{d}_j \geq \alpha T_r$$

where α is a specified tolerance level, T_i is the trace of $V_i V_i'$, $T_r = T_1 + \ldots + T_M$, ${}_i d_j$ are the eigenvalues of $V_i V_i'$, and the $\bar{d}_j$ are the eigenvalues of $\bar{Y}\bar{Y}'$, then we can approximate V by $\bar{V}$ at the $100\alpha\%$ level, where

$$\bar{V} = g_1 w_1 + \ldots + g_{\bar{k}} w_{\bar{k}} \qquad (12)$$

3.0 ESMR DATA IN POLAR RESEARCH

Passive microwave images of the polar regions obtained from the Nimbus-5 [3] ESMR brightness temperature measurements [4] have been shown to be a valuable source of polar information. The ESMR receiver (1.55 cm) is generally useful in all-weather all-season situations, and, in particular, is able to detect the large contrast between the brightness temperature of sea ice and the brightness temperature of open water. It is because of this contrast that the edge of the ice pack can be identified and information on sea ice concentration and ice type derived from these images. Scanning of the ESMR sensor provides complete spatial detail while continuous satellite coverage of these regions on a daily basis provides temporal detail (Zwally and Gloersen 1977).

Gloersen et al (1978) characterized the time variation of the sea-ice concentration and multi-year ice fraction within the pack ice in the Arctic Basin through analysis of the ESMR microwave images and other data acquired using the NASA CV-990 airborne laboratory. The data were analyzed for four seasons during 1973-1975. These observations have shown significant variations in the sea-ice concentration in the spring, late fall and early winter.

Carsey (1980) used the ESMR microwave images in a study of the long-term and short-term behavior of the Weddell Polynya for the years 1973-1977. This polynya or ice-enclosed open area was observed during the 1974, 1975, and 1976 winters. The behavior of this polynya margin and the regional ice concentration are interpreted in light of several oceanographic and meteorological theories explaining the circulation relevant to its origin, stability and role. He concludes that water column stability preconditioning alone is a necessary, but not sufficient condition for the existence of the polynya.

---

(3) The Nimbus-5 spacecraft was launched 11 December 1972 into a nearly circular polar orbit (1089 x 1102 km) permitting complete global coverage every 12 hours.

(4) The microwave radiation thermally emitted by an object is called its brightness temperature. It is expressed in units of temperature since the radiation emitted by a perfect emitter is proportional to its physical temperature for wavelengths in the microwave region. (Zwally and Gloersen 1977)

Crane et al (1982) used the ESMR data to determine the spatial and temporal patterns of change in microwave signatures of Arctic sea ice during a full annual cycle (1973/1974). Interactions of ice conditions with the atmosphere are examined using grid point data for surface air temperature and atmospheric pressure. An EOF/principal component analysis is used to examine the major elements present in the microwave and atmospheric data. Principal components from these analyses are then used in a canonical correlation analysis to determine interassociations present between the ice and atmosphere in the Beaufort Sea and the European sectors on a synoptic time scale.

Rayner and Howarth (1979) studied the areal extent and variability of Antarctic sea ice using the ESMR brightness temperatures from 19 December 1972 to 4 June 1975 for a total of 219 three-day time points with two data gaps (one from 26 February to 29 May 1973, the other from 1 August 1973 to 5 September 1973). The seasonal and interannual variations in Antarctic sea ice, e.g., the times of ice break-up and ice build-up, are important for fishing operations and coastal navigation. Also, these variations influence global climate.

In their method of analysis by Fourier decomposition Rayner and Howarth generate two series: one of maximum ice extent (minimum latitude or MINL) and one of minimum ice extent (maximum latitude or MAXL). Both these series with values at the integer longitudes follow the 155 K isotherm around the Antarctic continent and are assumed to coincide with the 15% ice-sea isopleth which they take to define the ice-sea boundary (Zwally et al 1976). Land masses are initially masked out. The reason for using two series is that quite frequently, due to polynyas and large embayments within the ice pack, the 155 K isotherm crosses the same meridian more than once. For a Fourier series representation of the ice-sea boundary the function must be single-valued as well as periodic.

For the 219 time points both the MAXL and MINL series (latitude of the 155 K brightness temperature isotherm versus integer longitude) were expanded in a Fourier series each containing 180

frequencies corresponding to the 360 longitudinal points. Results of their analysis reveal that the first seven harmonics are sufficient to account for more than 70% of the variance in the MINL boundary over the observation period and more than 90% of the variance during the winter seasons.

From their analysis of the amplitudes of the Fourier series with time they conclude that: (1) the time variation of the spatial mean latitude of the boundary is relatively smooth with a maximum occurring on 4 September 1974 and a minimum on 19 February 1975 (Figures 1 and 2); (2) the cold seasons are relatively long (205 days) and the summer season relatively short (160 days); (3) the time variation of the spatial mean latitude is asymmetric with the spring-summer removal of ice lasting 120 days and the autumn-winter increase lasting 150 days.

Cavalieri and Parkinson (1980) have used Rayner and Howarth's MINL series every ten degrees of longitude for the year 1974 and have compared the three-day averaged ESMR brightness temperatures with 1000 mb temperature and sea level pressure fields obtained from the Australian meteorological data set. In their work they also performed a Fourier decomposition - one on each of these three variables - and concluded that the first three harmonics were sufficient to account for most of the variance of the sea ice extent and temperature for any three-day period. Their results demonstrate an ice-atmosphere coupling of varying strength throughout the year.

Zwally et al (1981) have created a summary data set containing Antarctic sea-ice conditions derived from the ESMR brightness temperature measurements for the years 1973 through 1976. The measurements have been mapped onto a polar stereographic grid enclosing the 50°S latitude circle. Sea ice concentrations have been calculated from the data for each grid element with an algorithm which uses an emissivity of 0.9 and an ice physical temperature estimate from climatological surface air temperatures. Monthly, multi-year monthly, and yearly maps of brightness temperatures and sea ice concentrations have been created. In their work they conclude that the microwave

brightness temperatures of Antarctic sea ice are predominantly characteristic of first-year ice with an emissivity of 0.92 at the 1.55 cm wavelength of the ESMR.

A detailed analysis of Antarctic sea ice for the years 1973 through 1976 as derived from satellite passive microwave observations has been prepared (Zwally et al 1983) and is contained in an atlas which includes pseudo-color images of brightness temperature, sea ice concentration, changes in ice concentration, and multi-year average concentration.

3.1 EMISSIVITY, BRIGHTNESS TEMPERATURE, AND SEA ICE CONCENTRATION

The Nimbus-5 ESMR receiver has a center frequency of 19.35 GHz (1.55 cm) with an IF bandpass of from 5 to 125 MHz and is therefore sensitive to radiation from 19.225 to 19.475 GHz, except for a 10 MHz gap in the center of the band (Wilheit 1972). The radiometer is of the Dicke-type (Dicke 1946) with a temperature sensitivity of 2°K and is fed by a phased-array antenna consisting of 103 waveguide elements each having an electrical ferrite phase shifter which step-scans across the sub-satellite track in 78 positions. The total swath is $\pm$ 50° from nadir (Wilheit 1972, Gloersen et al 1973). Microwave images produced by the ESMR instrument have a spatial resolution of approximately 30 kilometers.

Radiation (or brightness temperature) at the 1.55 cm wavelength is directly proportional to the received radiometric power since the Rayleigh-Jeans approximation holds.(5) It is affected by high humidity and large water droplets in the atmosphere. Since the humidity is low and the number and size of water droplets are small in the south polar region, the received radiation can be assumed to be emitted from the earth's surface. Also, the radiation is not affected by darkness or cloud cover (Wilheit 1972, Wilheit et al 1972).

The basic equation for microwave radiometry is (Wilheit 1972, Zwally and Gloersen 1977)

$$T_B = \epsilon T \qquad (13)$$

where T_B is brightness temperature, ϵ is emissivity and T is the thermodynamic temperature of the emitting surface.

For microwave radiation of wavelength 1.55 cm, the emissivity of sea water is approximately 0.4, first-year sea ice approximately

---

(5) The Rayleigh-Jeans approximation for the intensity of thermal radiation from a blackbody works well at microwave frequencies (1-500 GHz) and at temperatures typical of the earth and its atmosphere (200 - 300°K) (Wilheit 1972).

0.95, and multi-year ice from 0.8 to 0.9 (Wilheit 1972; Gloersen et al 1973, 1974). More recent studies of first-year ice in the southern ocean have used a value of 0.92 for first-year sea ice emissivity (Zwally et al 1981).

For an area containing only first-year sea ice and open water, which is the case for most of the ice-influenced waters surrounding Antarctica, the brightness temperature T_B in a single instantaneous field of view (IFOV) is related to fractional ice concentration C (the fraction of the surface area within the IFOV which is covered by ice) by

$$T_B = \epsilon_o T_o C + (\epsilon_w T_w + A)(1 - C) \qquad (14)$$

where $\epsilon_o T_o$ is first-year sea ice brightness temperature (assumed to be 235 K), $\epsilon_w T_w$ is open water brightness temperature (assumed to be 120 K), and A is the brightness temperature contributed by atmospheric water vapor (assumed to be 15 K over open water areas and 0 over ice)(Zwally et al 1976; Zwally and Gloersen 1977). Neglecting variations of the ice physical temperature (T_o), substituting the foregoing approximate values into (14) and multiplying by 100 to express C in percent, we obtain

$$C = (T_B - 135)\% \qquad (15)$$

Equation (15) is accurate to approximately 15% over most of the Antarctic region where sea ice predominantly has the microwave emissivity of first-year ice even though in some regions it may be older than first-year ice (Zwally et al 1983).

4.0 ANALYSIS AND RESULTS

In Section 4.1, characteristics of the data set are discussed, such as the period of observation, spatial coverage, temporal and spatial resolution, and missing data points. The minimum and maximum ice extents during the period of observation are shown, as well as time series plots of the spatial mean vector, its associated spatial standard deviation, and power spectra of these functions.

In Section 4.2, the temporal mean and standard deviation ice brightness temperature maps for this time period are discussed. Characteristic features such as the Weddell Polynya, the edge of the pack ice, and the region occupied by ice year round, are identified. It is suggested that the advance and retreat of the ice edge over the annual cycle may be characterized by a conceptualy simple one-dimensional model with the gradient of mean ice concentration contours along a "growth/decay trajectory" on the mean map describing a nearly linear ramp function.

An EOF decomposition of the sea ice brightness temperature anomaly field is discussed in Section 4.3. Gray scale/contour maps of the first 10 EOF's are shown, along with their corresponding time coefficients (or principal components) and variance spectra of the latter. In the interpretation of the EOF's, the spatial pattern of anomalies over the entire grid of points can be considered to be a pattern of constructive and destructive interferences between the standing wave patterns in the EOF maps (Figures 6 through 10). In context with the one-dimensional model, the interference patterns between the EOF standing waves serve, in part, to reconstruct the advance and retreat of the step-like ice edge through the annual cycle of growth and decay. A physical interpretation of the first four EOF's and their coefficients and variance spectra is given.

In Section 4.4, the method of matrix partitioning in the time domain to approximate the "global" principal component structure is compared to the direct method of calculating global principal components. Calculations for the first three "pseudo" principal components are carried out for a tolerance level of 81% (i.e., retaining 81% of total sample variance) and are in good agreement with the first three global components.

4.1 DATA SET CHARACTERISTICS

An extensive time series of Nimbus-5 ESMR images has been processed at Goddard Space Flight Center. ESMR brightness temperatures accumulated during each 3-day period since 30 September 1973 were resampled to calculate 3-day average brightness temperatures at each of 293 x 293 grid points which are equally spaced when overlaid on the polar stereographic map projection illustrated in Figures 1 through 3. The average distance between grid points is approximately 30 km. The characteristics of this data set are more fully described by Zwally and Gloersen (1977).

For the present analysis, an ensemble of ESMR sea ice T_B maps was selected for the time period extending from 30 September 1973 through 25 May 1975. Of the 201 3-day time intervals spanning this 20 month sample period, 170 usable sea ice maps exist, and the 31 missing data points are distributed in relatively short time gaps: the largest gap spans 6 time points, another spans 5 points, and the rest are smaller. The missing data in the time domain were treated using the Fourier analysis methods described by Murray (1981).

The space domain selected for analysis was restricted to the 15,597 oceanic grid points falling within the box labelled "Area Analyzed" in Figures 1 through 3. The raw data vector, at any time point t, thus contains the 3-day average brightness temperature at each of these 15,597 grid points (arranged in a fixed order). Recalling equation (15), we may interpret each $(T_B - 135)$ as ice concentration in percent at time t and the associated grid point. Missing data at individual grid points within any given map were filled by interpolating linearly over time at that location.

Figures 1 and 2 illustrate the positions of the ice edge, during this ensemble period, at the respective times of maximum and minimum sea ice extent (after Rayner and Howarth 1979). T_B variations at open ocean grid points seaward of the maximum ice extent (Figure 1) are associated with atmospheric water vapor

and liquid water droplets in passing weather systems. These signals typically range from 5 to 10 Kelvins. Figure 3 illustrates the geography of the Antarctic Continent, major glaciers, continental ice sheets, various islands, and South America, in relation to the oceanic area covered by the ensemble grid.

The fraction of the total analysis area covered by sea ice at any given time may be estimated approximately by averaging each data vector over the 15,597 grid points. The time series of the spatial mean vector and the associated time series of spatial standard deviations are plotted in Figure 4. Also illustrated in Figure 4 are the least squares power spectra of these series (Vanicek 1969, 1971; Wells and Vanicek 1978; Murray 1981). Both the spatial mean and spatial standard deviation are dominated by the annual cycle with a significant spectral peak associated with a half-year period. At the time of maximum ice extent, approximately 40% to 45% of the total oceanic area within the analysis area (Figure 3) is ice-covered. At the time of minimum ice extent, approximately 5% to 8% is ice-covered, using the approximation that $(T_B - 135)$ is ice concentration in percent.

4.2 TEMPORAL MEAN AND STANDARD DEVIATION OF SEA ICE BRIGHTNESS TEMPERATURE IN THE WEDDELL SEA (9/30/73 - 5/25/75)

The temporal mean and standard deviation ice brightness temperature maps for this time series are illustrated in the top two panels of Figure 6. The 154 K mean brightness temperature isotherm and isoline of 14 K standard deviation correspond closely to the maximum ice extent (Figure 1). The open ocean region seaward of the maximum ice extent is characterized by an average brightness temperature slightly greater than 135 K, together with a standard deviation of approximately 10 K due to water vapor and liquid water in weather systems (Allison et al 1974; Wilheit et al 1975; Zwally and Gloersen 1977).

The region occupied by sea ice year round, just to the east of the Antarctic Peninsula, is characterized by a high average brightness temperature and also a standard deviation of only $10^{o}K$.

The 200 km x 1000 km area of low average brightness temperature near 0^{o} longitude is a persistent, major polynya which has been studied by several investigators and called the "Weddell Polynya" (Zwally and Gloersen 1977; Rayner and Howarth 1979; Carsey 1980; Parkinson 1983). The ice pack completely covered the Weddell Polynya in the winter of 1973, but during the winters of 1974 and 1975 this region was primarily open water with ice concentrations rarely exceeding 15% (bottom panel of Figure 11). Variation in ice concentration in this vicinity in 1974 was primarily due to a gradual change in shape of the polynya from August through November 1974 (Carsey 1980). The standard deviations of grid points within the Weddell Polynya are corresponding low, being only slightly greater than those of the open sea beyond the maximum ice extent.

The Weddell Polynya lies along the locus of the Antarctic Divergence, as it projects into the Weddell Sea. Enhanced divergent wind stress, due to inversion winds off the ice shelf, are thought to produce enhanced upwelling of warm deep water in this region and thus maintain the polynya as an open water area (Zwally et. al 1976; Zwally and Gloersen 1977).

Parkinson (1983), using mean climatological data as input, has successfully simulated a Weddell polynya through a sequence of numerical simulations of the ice cover, and concludes, "... the model obtains a full-scale, 0% concentration Weddell polynya which can be moved and prolonged by changing the wind forcing. Results seem to suggest that the Weddell polynya might arise in response to the winds, but then is maintained through oceanographic factors, including possibly a wind-driven divergence, or through the joint influence of the ocean and such feedbacks as the atmospheric warming which the polynya would be expected to induce."

In the mean field, the curved tongue-like protuberance emanating eastward from the Antarctic Peninsula represents the path of maximum growth and decay of the ice pack over the annual cycle. For purposes of discussion, the dashed line down the center of this tongue will be referred to as the ice "growth/decay trajectory". The gradient of mean ice concentration contours along the growth/decay trajectory may be characterized as a nearly linear ramp function. The ice growth/decay trajectory curves around the Weddell Polynya, reflecting the low average ice concentration there, even though it closed over in 1973.

The ramplike nature of the mean T_B contours along the growth/decay trajectory can be readily explained in terms of a simple one-dimensional model. Consider a horizontal axis from $x = 0$ to $x = 1$, along which ice concentration $C(x,t)$ at any time t may be either 0 (open water) or 1 (ice). At time $t = 0$, $C(0,0) = 1$ and $C(x,0) = 0$ for $x > 0$. Over some period T, the ice edge is observed to advance from $x = 0$ (at time $t = 0$) at a uniform speed to arrive at $x = 1$ at time $t = T/2$, and then to retreat at the same rate, returning to the initial conditions at time $t = T$. If we consider the mid-point at $x = 0.5$, $C(0.5,t)$ is 0 for half of the cycle and 1 for the other half, with a mean (over T) of $\overline{C}(0.5) = 0.5$. Similar consideration of the mean at a few other points quickly reveals that $\overline{C}(x)$ is a linear ramp function sloping from $\overline{C}(0) = 1$ to $\overline{C}(1) = 0$. The mean concentration in this simple model is obviously similar to the contour gradient along the ice growth/decay trajectory in the mean ice concentration field (Figure 6).

If we now consider the standard deviation associated with the above one-dimensional model, $S_C(x) = \sqrt{x(1-x)}$, we obtain for a few selected points: $S_C(0) = S_C(1) = 0$, $S_C(.25) = S_C(.75) = 0.433$, $S_C(.5) = 0.5$. This is, therefore, a symmetric function with steep slopes near $x = 0$ and $x = 1$, and a broad maximum at $x = 0.5$. Again, there are obvious similarities between the standard deviation curve of the model and the contours of standard deviation in sea ice brightness temperatures along the growth/decay trajectory (upper right panel of Figure 6).

From the above qualitative comparisons of geometric characteristics between the modeled and observed sea ice T_B means and standard deviations, we may conclude that much of the observed variance may be explained by analogy to a simple "advancing step function" model of the ice pack. This interpretation is also supported by the time sequences of ice concentration at selected individual pixels within the region influenced by the ice pack (Figure 11). In all three cases shown here, the transition from open water to ice-covered (and vice versa) occurs abruptly. Near the center of the pack, the ensemble average ice concentration - again approximated as $(T_B - 135)\%$ - is close to 50%. And, at the pixel near the ice edge, the ensemble average ice concentration is only a few percent. When we consider the EOF decomposition of sea ice brightness temperature anomalies from the sample mean (Section 4.3 below), it will therefore be helpful to think in terms of reconstructing a progressive, slab-like advance and decay sequence through interference between "standing wave" EOF patterns, in combination with a linear mean slope extending from minimum to maximum ice extent.

4.3 EOF DECOMPOSITION OF SEA ICE BRIGHTNESS TEMPERATURE ANOMALIES IN THE WEDDELL SEA (9/30/73 - 5/25/75)

The usual objective of EOF analysis of geophysical observations is to rotate the representation of the data to distances along a few p-dimensional directions containing most of the observed signal. This geometrical perspective is discussed in more detail here in Appendix A and elsewhere in many of the references cited above in Section 1. If the original p-dimensional measured variables are truly random and uncorrelated with each other, then there will be no dominant dispersion (variance) directions and EOF analysis becomes a fruitless exercise. It is more frequently the case with geophysical observations, however, that strong correlations exist between the original variables (the measurement of these variables being made independently), so that preferred variance directions do exist and can be illuminated through EOF

decompositions. Stated another way, EOF methods are often useful in situations where all p measurables respond to variations in some common forcing function, such as seasonal variation in solar radiative flux. The projections of the individual responses onto linear combinations of the original measurables (each such combination being a rotated direction) will influence the EOF coordinates according to the importance of that process in the physical system being studied.

In the case at hand, the original p dimensions are raw brightness temperatures at the 15,597 spatial grid points. A "direction" in this coordinate frame thus would be displayed graphically, either as a curve (if all grid points were indexed and plotted on a single abscissa with T_B as the ordinate) or as a two-dimensional gray scale/contour plot where the grid points are located on a map projection. The original measurement origin is thus located at zero brightness temperature at all grid points, a position far from the "centroid" of the sample, as given by the sample mean (upper left panel of Figure 6). Before rotating to find principal axes of brightness temperature variations, it is therefore necessary to center the data matrix by subtracting the temporal mean from each observation. In geometric terms, this amounts to translating the origin to the position of the sample mean or centroid of the data. The resulting data matrix V in (1) thus contains column vectors of brightness temperature anomalies, v_j, relative to the temporal mean, for 170 time points. These anomaly values, in Kelvins, are now directly interpretable as ice concentration anomalies in percent.

The EOF's defining the principal directions of anomaly variations in ice concentration are the eigenvectors of the spatial sample covariance matrix

$$\hat{S} = VV'/(q-1) = VV'/169$$

where q = 170 is the sample size in the time domain.

Since the mean is subtracted from each observation there are at most 169 degrees of freedom and, therefore, the rank of $\hat{S}$, or the number of nonzero eigenvalues, is less than or equal to 169.

The elements along the main diagonal of $\hat{S}$ are the sample variance of brightness temperature measurements at each associated spatial grid point. Therefore, the square roots of these elements yield the sample standard deviation shown as a gray scale/contour map in the upper right panel of Figure 6 and discussed in Section 4.2. The trace of $\hat{S}$ (sum of all the elements along the main diagonal) is total sample variance, a quantity which is invariant under the rigid axis rotations associated with a complete EOF decomposition (Section 2 and Appendix A).

In order to reduce computation time and storage requirements, the eigenvalues and eigenvectors of $\hat{S}$ were calculated by first determining the eigenstructure of the smaller time domain scatter matrix V'V which has the same eigenvalues as VV'. The desired spatial eigenvectors and temporal principal components were then obtained as explained in Section 2 and Appendix B.

A determination that only the first k eigenvalues are statistically greater than zero amounts to a statement that the first k principal components represent signal, and the remainder represent noise. Preisendorfer et al (1982) have recently reviewed this topic and provide a systematic set of rules for selecting significant eigenvalues, but ambiguities remain even so.

One family of eigenvalue selection rules is based on slope variations in a plot of the logarithm of eigenvalue (LEV) versus eigenvalue number. Craddock and Flood (1969) and Craddock and Flintoff (1970), for example, truncate the "signal" eigenvalues at the point beyond which the LEV curve may be approximated by a straight line. Other criteria for determining truncation level include retention of eigenvalues exceeding 1% of the total sample variance (Kaiser 1960), retaining only eigenvalues which are "much larger than others" (Beale et al 1967), retention of eigenvalues which cumulatively account for 99% of the total sample variance (Mueller 1976), and subjective determinations based on inspection of the LEV diagram (Rinne and Järvenoja 1979). In all cases, some

element of subjective interpretation is involved in the truncation decision.

The LEV diagram of the sea ice covariance matrix $\hat{S}$ is plotted in Figure 5. By the Craddock et al criterion, the first 85 EOF's should be retained to provide a "complete" decomposition of the sea ice anomaly field. This truncation level would retain 98.92% of total sample variance. The first 10 eigenvalues of $\hat{S}$ and their respective and cumulative contributions to the total sample variance are compiled in Table 1. Each eigenvalue equates to variance in the principal component (distance) in the direction defined by the associated eigenvector (EOF). Nearly 92% of total sample variance in ice concentration is resolved by a principal component representation in these 10 directions. By using either Craddock's criterion or Mueller's we would retain the first 85 EOF's. By neglecting those eigenvalues which individually account for less than 1% of total variance we would retain only the first 7 EOF's.

The issue of truncation would become critical in a study which used a truncated EOF decomposition of the data in conjunction with a numerical sea ice model, or in the calculation of cross-covariance spectra between truncated representations of sea ice concentration and another variable, such as atmospheric pressure. Truncation is less critical in purely descriptive analyses of organized structure in space/time variability associated with a geophysical field. The present analysis is arbitrarily confined to a descriptive presentation and interpretation of the first 10 EOF's and principal components of sea ice concentration anomalies in the Weddell Sea. Furthermore, detailed discussions focus primarily on only the first 4 EOF's, which are assumed to represent the dominant normal modes of variation in the field.

The first 10 EOF's are illustrated as gray-scale/contour maps in Figures 6 through 10. Shown beside each EOF map are the corresponding principal component and the variance spectrum of the principal component time series. In all EOF maps, major anomaly amplitudes are confined to grid points falling between the maximum ice extent boundary and the shoreline of Antarctica. In

many of the EOF's, very small amplitude anomaly patterns occur over the open ocean areas beyond the maximum ice boundary. These anomalies are due to water vapor and liquid water fluctuations along the storm tracks through this region during this ensemble period.

The kth principal component at any time t represents the amplitude of the normalized (unit length) spatial anomaly pattern illustrated in the kth EOF map. The interplay between an EOF and its time varying principal component can be most easily understood through a specific example. Examine EOF/principal component #2 (Figure 6) and note that the EOF pattern indicates a negative anomaly of < -0.016 at position (60°S, 15°E) and a positive anomaly of +0.012 at position (65°S, 40°W). On day 250, the 2nd principal component has an approximate value of +2000 K, which yields 2nd EOF anomaly contributions of < -32 K at (60°S, 15°E) and +24 K at (65°S, 40°W). Conversely, on day 400 the 2nd principal component has an approximate value of -1000 K, yielding 2nd EOF contributions of > 16 K at (60°S, 15°E) and -12 K at (65°S, 40°W). Reconstruction of the time modulation of the overall brightness temperature anomaly at these two locations requires, of course, that the contribution of all significant EOF's be summed. Thus, the spatial pattern of anomalies over the entire grid can be considered to be a pattern of constructive and destructive interferences between the standing wave patterns in the EOF maps(Figs 6-10).

Recall now the discussion of the simple one-dimensional "advancing step function" model introduced in Section 4.2 above. In the context discussed there, the interference patterns between EOF standing waves serve, in part, to reconstruct the advance and retreat of the step-like ice edge through the domain influenced by growth and decay of sea ice through the annual cycle. The abrupt transition from water to ice (and the reverse) observed at individual pixels (Figure 11) is consistent with this interpretation.

In general, the 1st EOF and principal component describe a long wavelength modulation of positive and negative anomalies, following a spatial pattern which is qualitatively similar to the shape of the standard deviation of the one-dimensional model (Section 4.2). Near the time of maximum ice extent (Rayner and Howarth 1979), the

1st EOF anomaly monotonically increases T_B relative to the mean, with maximum contributions near the center of the ice pack. Conversely, near the time of minimum ice extent, the 1st EOF anomalies are monotonically negative and tend to reduce T_B over the ice-influenced region towards the uniformly low values associated with open water.

The 1st principal component varies smoothly between times of minimum and maximum sea ice coverage in concert with previously published descriptions of the annual cycle of ice growth and decay in the Weddell Sea (Rayner and Howarth 1979; Zwally and Gloersen 1977). Not surprisingly, therefore, the variance spectrum of the 1st principal component is dominated by the annual cycle, with smaller spectral peaks associated with a half-year period and a 120 day period. (The occurrence of peak power at 348 days, rather than 365 days, is almost certainly an artifact of the ensemble period being only 20 months. This series is too short to allow accurate estimates of a variance spectrum dominated by a 12-month cycle.)

The 2nd principal component time series is phase shifted from the 1st in such a way that interferences between 1st and 2nd EOF anomaly patterns will improve the representation of the advance and retreat of the ice edge during periods of growth and decay (Figure 6). A similar conclusion may be drawn from inspection of interactions between the first EOF/principal component and numbers 3 and 5 through 10. In each case the largest principal component amplitudes (+ or -) occur during periods of ice growth and/or decay. Also, in each case the dominant spatial pattern in the higher EOF may be seen to produce interferences with the pattern of the mean and 1st EOF which reproduce a step-like manifestation of the ice edge.

Many of the strongest anomaly patterns occur in regions where the ice pack undergoes extremely rapid growth and decay during the transition phases. This can be seen by comparing the EOF anomalies,

in this light, with 1974 monthly average sea ice extent contours published by Cavalieri and Parkinson (1981) and included here as Figure 12. During the ice pack growth period in March through May, the spacing between monthly contour intervals is large in the western and central areas of the Weddell Sea (Figure 12a). Compare this especially with the anomaly patterns in the 2nd and 3rd EOF's and the rapid positive growth in their principal components during this period (Figures 6 and 7). Then, during the early retreat of the ice pack in November and December, a large contour interval outlines the rapid expansion of the polynya, followed by an abrupt retreat to nearly minimum extent in January 1975 (Figure 12b). The breakup of the pack ice followed a more complex sequence of spatial patterns than did the ice growth, and is manifested by rapid positive to negative excursions in most of the principal components (Figures 6 - 10).

EOF #4 and its principal component time series (Figure 7) uniquely represent interannual variability in the Weddell Polynya between 1973 and 1974. In the winter of 1973, when the polynya was absent until early in the spring breakup of the ice pack, positive brightness temperature anomalies prevailed here. Then, in 1974, the polynya remained open throughout the winter, creating a negative T_B anomaly relative to the 20-month mean. The anomaly amplitudes in EOF #4 also indicate a more subtle effect associated with the band of -0.012 anomaly extending zonally eastward from the tip of the Antarctic Peninsula (Figures 3 and 7). In 1973, when the 4th principal component had a large positive value (polynya absent), the maximum ice extent boundary in these longitudes was displaced anomalously to the south. In 1974, when the 4th principal component had a large negative value (polynya present), the maximum ice extent boundary was displaced anomalously to the north. A much longer time series must be analysed to determine whether there is significant evidence of an association between presence of the Weddell Polynya and maximum ice extent. In the present sample this apparent association could be a purely coincidental contrast between two winters.

The primary roles of EOF's 2,3, and 5 through 10 in reconstructing the movement of the ice edge during growth and decay phases is

also manifested in the time histories of each principal component's percentage contribution to the spatially averaged mean squared anomaly (equation (8) and Figures 13 and 14). The 1st EOF dominates the mean squared anomaly during periods of both maximum and minimum ice extent and falls abruptly during growth and decay phases. At the times of ice minima, contributions from EOF's 2 through 10 are negligible. During the periods of maximum ice cover EOF #4 is a significant contributor, representing the markedly different manifestations of the Weddell Polynya in 1973 and 1974. The situation is quite different during the ice growth and decay phases. The mean squared contribution of principal component #1 falls steeply to zero, and then rises just as steeply, as the sign of the principal component reverses. Coincident with these "notch-like" signatures, the mean squared anomaly signals associated with principal components 2,3, and 5 - 10 appear as sharp pulses of energy. During each such pulse, the shorter wavelength anomaly patterns of the associated EOF's make strong contributions to the reproduction of the ice edge.

The variance spectra of the first 10 principal components are all dominated by peaks associated with periods which are a significant fraction of the approximate 600 day ensemble period. As previously mentioned, this time series is much too short to attribute a high degree of accuracy to the spectra illustrated in Figures 6 through 10. Nevertheless, the dominant peaks can be clearly associated with well-known processes, including the 365 day (0.003 day^{-1}) annual cycle (particularly in spectra of principal components 1 and 2), a 160 day (0.006 day^{-1}) warm season and 205 day (0.005 day^{-1}) cold season (Zwally and Gloersen 1977; Rayner and Howarth 1979), and a 120 day (0.008 day^{-1}) period of ice removal (Rayner and Howarth 1979).

4.4 EOF COMPUTATIONS USING PARTITIONS IN THE TIME DOMAIN

It was noted in Section 4.3 that the actual EOF computations were done using the smaller time-domain scatter matrix V'V, and the results transformed for application to the spatial covariance matrix $\hat{S}$ using the relationships explained in Section 2 and Appendix B. The 170 x 170 matrix V'V is small enough to allow practical direct computation of its eigenvalues and eigenvectors using standard computer subroutines. Were sample size to grow much larger, however, direct eigenvalue computations would become impractical and the techniques outlined for separate computations of eigenvectors and eigenvalues of smaller partitions, and subsequent joining of the results (Appendices C and D) would become essential. Therefore, this data set was used to test the accuracy of global principal components estimated by joining truncated sets of principal components associated with the smaller dimensioned scatter matrices.

The data matrix (V) was partitioned in the time domain into 5 sub-matrices, each of dimension 15,597 x 34 and the eigenstructure of each of the 34 x 34 $V_i'V_i$ ($i = 1,..,5$) scatter matrices determined. Using the joining procedure outlined in Appendices C and D and retaining 81% of the total sample variance, a truncated set of 9 principal components (and associated EOF's) from all these partitions was joined to approximate the global principal component structure. These approximations (or pseudo-principal components) were then compared with the global principal components calculated directly without truncation. The first three pseudo-principal components are plotted as open circles in Figure 6 and 7. The 1st pseudo-principal component series is virtually indistinguishable from the directly computed one, and the comparisons are nearly as good for the 2nd and 3rd principal components. Clearly, this approach will be usable, given proper retention of total sample variance in the truncated computations, for obtaining accurate estimates of at least the lower ordered EOF's from indefinitely large ensembles of sea ice brightness temperatures.

A similar computation was carried out by partitioning the spatial grid into three longitudinal sectors. Equally good approximations to the global EOF's were obtained with this approach to partitioning of the sample. The results from the spatial partition computations allow some interesting comparisons to be made concerning the global importance of locally important anomaly patterns, particularly in the higher ordered EOF's. However, that type of interpretation is beyond the scope of the present paper, and the results of spatial partition computations will not be presented here.

5.0 DISCUSSION AND CONCLUSIONS

A matrix partitioning scheme has been presented for approximating the eigenstructure of a large sample covariance matrix. The data array, a field of measured anomalies (of some physical variable) relative to their time averages, may be partitioned in either the time domain or the space domain. Eigenvectors of the smaller dimensioned covariance matrices associated with the partitioned data sets (and their principal components) may be calculated independently and joined to approximate the eigenstructure of the larger covariance matrix associated with the unpartitioned data set. The accuracy of the desired approximation (in terms of retaining a given percent of total sample variance) and the magnitudes of the largest eigenvalues from the partition covariance matrices determine the number of local EOF's (eigenvectors) and principal components to be used in the joining process.

This method is shown to allow accurate estimation of spatial EOF's for time series of satellite image data where there is a large number of spatial grid points. The spatial covariance matrix associated with any ensemble of satellite images is far too large to allow direct computation of its eigenvalues and eigenvectors, the latter being the desired spatial EOF's. In many cases, however, the number of images in an ensemble (its time dimension) is sufficiently small to permit direct computation of the eigenvalues and eigenvectors of the temporal scatter matrix. The latter eigenvectors can be easily transformed to obtain the eigenvectors of the spatial covariance matrix. As a result, great computational savings are realized.

There are a number of satellite data ensembles where the dimensions of both the time and space scatter matrices are too large to permit direct computation of the eigenstructure of either matrix. In such cases, the above mentioned matrix partitioning scheme must be employed to break the computational problem into manageable pieces. The methods by which the partition results are joined are described in detail in Appendices C and D.

The accuracy and efficiency of the partitioning approach were

tested using a 20-month ensemble of Nimbus-5 ESMR measurements of sea ice brightness temperature emissions in the Weddell Sea. The time series of sea ice T_B maps extended from 30 September 1973 through 25 May 1975 and included 170 3-day composite average maps (leaving 31 reasonably well distributed time gaps). The spatial representation was restricted to 15,597 oceanic grid points in the Weddell Sea and adjoining Antarctic Circumpolar Current regime. Spatial EOF's were first computed directly, using the 170 x 170 time scatter matrix as a computational expedient. Then, the first 3 EOF's were computed indirectly using partitioning in the time domain, and in another case, the space domain. Both partitioning methods yielded comparable results and the calculated EOF's and principal components agree remarkably well with those computed directly. It is concluded that this method is extremely well suited for analysis of data sets much larger than the one examined here.

The first 10 spatial EOF's, together, explain 92% of total sample variance in sea ice brightness temperature (or percent ice concentration) anomalies relative to the ensemble mean. The mean and standard deviation are shown, by qualitative comparison with a simple 1-dimensional model, to be consistent with those of a conceptual model of the ice pack as a 2-dimensional, quasi-uniform slab which grows and shrinks in spatial extent over the annual cycle of ice growth and decay. In this context, the dominant anomaly patterns in the spatial EOF's and the phase relationships of the principal components may be interpreted as a standing wave decomposition of the advance and retreat of the ice edge. At any time between maximum and minimum extent, the ice edge is represented by a linear pattern of interference between the ensemble mean ice concentration and the standing wave anomaly patterns in the EOF fields as modulated in amplitude by the time-varying principal components.

The fourth EOF/principal component uniquely accounts for the interannual difference in the Weddell Polynya, which was absent during the winter of 1973 and present throughout 1974. This interannual contrast accounts for 3% of total sample variance which is a highly significant fraction. Recall that the full variance associated with the annual cycle is present in the covariance matrix analyzed here! The spatial anomaly pattern in the fourth EOF also

shows that the presence of the polynya in 1974 was accompanied by an anomalous northward protrusion of the maximum ice extent, and the reverse in 1973 when the polynya was absent. A much longer time series would be needed to determine whether this apparent association of the polynya with maximum ice extent east of the Antarctic Peninsula occurs regularly, or was merely a coincidental artifact of the two years examined.

Power spectral analysis of the principal components reveal periods which can be related to the seasonal cycle of sea ice growth and decay in the Weddell Sea, harmonics of this cycle, the cold season (205 days), the warm season (160 days), and the duration of spring-summer ice removal (120 days) as reported in the literature.

The first four EOF's and their components can be considered the dominant or principal modes of variation in the ice field, accounting for 85% of the total information content in the data (field variance).

ACKNOWLEDGEMENTS

The authors express their appreciation to Dr. Donald J. Cavalieri (Code 912.1) and to Dr. David Fischel (formerly with Code 932) of the Goddard Space Flight Center for many valuable discussions, to Dr. Josefino C. Comiso (Code 912.1) for providing them with a sea/land data set for masking out land areas, and to Ms. Margo Osborne of Science Applications and Research (SAR) for helping them process the gray scale/contour EOF maps. The authors also wish to express their appreciation to Dr. Robert F. Cahalan (Code 910) for citing the basic reference by Yakovleva et. al (1968) for citing the basic reference by Yakovleva et. al (1968) for joining local EOF's and principal components.

REFERENCES

Alishouse, J.C., L.J. Crone, H.E. Fleming, F.L. Van Cleef and D.Q. Wark, 1967: A discussion of empirical orthogonal functions and their application to vertical temperature profiles. Tellus 19, pp 477-482.

Allison, L.J. et. al., 1974: Tropical cyclone rainfall as measured by the Nimbus-5 Electrically Scanning Microwave Radiometer. By L.J. Allison, E.B. Rodgers, T.T. Wilheit, and R.W. Fett. Bulletin of the American Meteorological Society, Vol. 55, No. 9, pp 1074-1089.

Anderson, T.W., 1958: An Introduction to Multivariate Statistical Analysis, John Wiley and Sons, Inc., New York. Chapter 11.

Anderson, T.W., 1963: Asymptotic Theory for principal component analysis. Ann. Math. Statistics, Vol. 34, pp 122-148.

Barnett, T.P., 1978: Estimating variability of surface air temperature in the Northern Hemisphere. Mon. Wea. Rev., 107, 1353-1367.

Barnett, T.P., and R.W. Preisendorfer, 1978: Multifield analog prediction of short-term climate fluctuations using a climate state vector. J. Atmos. Sci., 35, No. 10, 1771-1787.

Barnett, T.P., and K. Hasselmann, 1979: Techniques of linear prediction with application to oceanic and atmospheric fields in the tropical Pacific. Rev. Geophys. Space Phys., 17, 949-968.

Bartlett, M.S., 1954: A note on the multiplying factor for various χ^2 approximations. J. Royal Statistical Society, Vol B16, 296-298.

Beale, E.M.L., M.G. Kendall, and D.W. Mann, 1967: The discarding of variables in multivariate analysis. Biometrika, Vol 54, p 357.

Bodin, Svante, 1974: The use of empirical orthogonal functions in quasi-geostrophic numerical prediction models. Tellus 26.

Buell, C.E., 1972: Integral equation representation for factor analysis. J. Atm. Sci., Vol 28, pp 1502-1505.

Buell, C.E., 1975: The topography of the empirical orthogonal function. 4th Conference on Probability and Statistics in Atmospheric Sciences, Nov 18-21, Tallahassee, Fla., pp 188-193.

Buell, C.E., 1978: The number of significant proper functions of two-dimensional fields. J. App. Meteor., Vol 17, No. 6, 717-722.

Buell, C.E., 1979: On the physical interpretation of empirical orthogonal functions, 6th Conference on Probability and Statistics in Atmospheric Sciences, Oct 9-12, Banff, Alta. Canada.

Carsey, F.D., 1980: Microwave observation of the Weddell Polynya, Mon. Wea. Rev., Vol 108, pp 2032-2044.

Cavalieri, D.J., C.L. Parkinson, 1981: Large-scale variations in observed antarctic sea ice extent and associated atmospheric circulation. Mon Wea Rev, Vol 109, No. 11, pp 2323-2336.

Choi, S.C., 1967: Principal component analysis of seismic data and direction of the principal component for seismic record. Prepared for Air Force Technical Applications Center, Measurement Analysis Corporation, under project VELA UNIFORM, sponsored by ARPA, Seismic Data Laboratory Report No. 181.

Craddock, J.M., and C.R. Flood, 1969: Eigenvectors for representing the 500 mb geopotential surface over the Northern Hemisphere, Quart. J. Roy. Met. Soc., Vol 95, pp 576-593.

Craddock, J.M., and S. Flintoff, 1970: Eigenvector representations of Northern Hemispheric fields, Quart. J. R. Met Soc., Vol 96, pp 124-129.

Craddock, J.M., 1973: Problems and prospects for eigenvector analysis in meteorology. The Statistician, Vol 22, pp 133-144.

Crane, R.G., R.G. Barry, and H.J. Zwally, 1982: Analysis of atmosphere sea ice interactions in the Arctic Basin using ESMR microwave data, International Journal of Remote Sensing, Vol 3, No 3, pp 259-276.

Darroch, J.N., 1965: An optimal property of principal components, Ann. Math. Stat. 36, pp 1579-1582.

Davis, R.E., 1976: Predictability of sea surface temperature and sea level pressure anomalies over the North Pacific Ocean, Journal of Physical Oceanography, Vol 6, No 3, pp 249-266.

Davis, R.E., 1978: Predictability of sea level pressure anomalies over the North Pacific Ocean, Journal of Physical Oceanography, Vol 8, pp 233-246.

Dicke, R.H., 1946: The measurement of thermal radiation at microwave frequencies, Rev. Sci. Instr., Vol 17, p 280.

Frisch, R., 1929: Correlation and scatter in statistical variables, Nordic Stat. J., 1, pp 36-102.

Fukuoka, A., 1951: A study on 10-day forecast (a synthetic report), The Geophys. Mag. (Tokyo), 22, pp 177-288.

Garrilin, B.L., 1965: On the description of vertical structure of synoptical processes, Izv. Atm. and Oceanic Phys. Sc., Vol 1, No. 2, pp 8-12, translated by C.M. Wade.

Gilman, D.L., 1957: Empirical orthogonal functions applied to thirty-day forecasting. Sci. Rep. No. 1, Contract AF-19(604)1283, Dept. Meteor., MIT, 129 pages.

Girshick, M.A., 1936: Principal components. J. Amer. Statist. Assoc., vol 31, pp 519-528.

Gloersen, P., W. Nordberg, T.J. Schmugge, T.T. Wilheit, W.J. Campbell, 1973: Microwave signatures of first-year and multi-year sea ice. Journal of Geophysical Research, Vol 78, No. 18, pp 3564-3572.

Gloersen, P., T.T. Wilheit, T.C. Chang, and W. Nordberg, and W.J. Campbell, 1974: Microwave maps of the polar ice of the earth. Bull. Amer. Meteor. Soc., Vol 55, pp 1442-1448.

Gloersen, P. et. al, 1978: Time-dependence of sea-ice concentration and multi-year ice fraction in the Arctic Basin. By P. Gloersen, H.J. Zwally, A.T.C. Chang, D.K. Hall, W.J. Campbell, R.O. Ramseier. Boundary-Layer Meteorology 13, 339-359. , D. Reidel Publishing Company, Dordrecht, Holland.

Golub, G.H., and C. Reinsch, 1970: Singular value decomposition and least squares solutions. Numerical Math. 14, pp 403-420.

Good, I.J., 1969: Some applications of the singular decomposition of a matrix. Technometrics, Vol 11, No 4, pp 823-831.

Grimmer, M., 1963: The space filtering of monthly surface temperature anomaly data in terms of pattern using empirical orthogonal functions. Quart. J.R. Meteor. Soc., 89, pp 395-408.

Holmstrom, L., 1963: On a method for parametric representation of the state of the atmosphere. Tellus 15, pp 127-149.

Hotelling, H., 1933: Analysis of a complex of statistical variables into principal components. J. Educ. Psych., 24, pp 417-441, pp 498-521.

Jalickee, J.B., and W.J. Klepczynski, 1977: A method for compacting navigation tables. Navigation 24, pp 182-184.

Kaiser, H.F., 1960: The application of electronic computers to factor analysis. Educational and Psychological Measurements, 20, pp 141-151.

Kendall, M.G., 1957: A Course in Multivariate Analysis. Charles Griffin and Company, London.

Kendall, M.G., 1975: Multivariate Analysis. Hafner Press, New York.

Kidson, J.W., 1975: Eigenvector analysis of monthly mean surface data. Mon Wea Rev, 103, No 3, pp 177-186

Koprova, L.I., and Malkevich, M.S., 1965: On the empirical orthogonal functions for the optimal parameterization of temperature and humidity profiles. Izv., Atm. and Oceanic Phys. Ser., Vol 1, No 1, pp 27-32, translated by C.M. Wade.

Kshirsagar, A.M., 1972: Multivariate Analysis. Marcel Dekker, Inc., New York.

Kullbach, S., 1959: Information Theory and Statistics. John Wiley and Sons, New York.

Kutzbach, J.E., 1967: Empirical eigenvectors of sea level pressure, surface temperature and precipitation complexes over North America. J. Appl. Meteor., 6, 791-802.

Kutzbach, J.E., 1970: Large-scale features of monthly mean Northern Hemisphere anomaly maps of sea-level pressure. Mon Wea Rev, 98, 708-716.

Lawley, D.N., 1956: Test of significance for the latent roots of covariance and correlation matrices. Biometrika, 43, 128-136.

Lorenz, E.N., 1956: Empirical orthogonal functions and statistical weather prediction. Sci. Report No. 1, Dept. of Meteorology, MIT.

Marchuk, G.I., 1965: On the role of studies of the physics of the atmosphere and the oceans in weather forecasting. Izv., Atm. and Oceanic Phys. Ser., Vol. 1, pp 5-7, translated by C.M. Wade.

Marriott, F.H.C., 1974: The interpretation of multiple observations, Academic Press, London, New York, San Francisco.

Mateer, C.I., 1965: On the information content of Umkehr observations, J. of Atm. Sci., 22, 370-381.

Miesch, A.T., 1980: Scaling variables and interpretation of eigenvalues in principal component analysis of geologic data, Math. Geol., Vol 12, No. 6, pp 523-538.

Mueller, J.L., 1976: Ocean color spectra measured off the Oregon coast, Applied Optics.

Murray, C.W., 1980: Calculation of power spectrums from digital time series with missing data points. NASA TM 82016.

Noble, B., and J.W. Deanial, 1977: Applied Linear Algebra, 2nd edition, Prentice Hall.

North, G.R., T.L. Bell, and R.F. Cahalan, 1982: Sampling errors in the estimation of empirical orthogonal functions, Mon Wea Rev 110, 699-706.

Obukhov, A.M., 1960: The statistically orthogonal expansion of empirical functions. Izv. Geophys. Ser. 1960, pp 432-439, translated by F. Goodspeed.

Okamoto, Masashi, and M. Kanazawa, 1968: Minimization of eigen values of a matrix and optimality of principal components. Ann Math. Statist., V 39, no. 3, pp 859-663.

Parkinson, Claire L., 1983: On the development and cause of the Weddell Polynya in a sea ice simulation. J. Phy. Ocean, V.13 pp 501-511.

Pearson,K. 1901: On lines and planes of closest fit to systems of points in space. Phil. Mag., 2 (Sixth Series)pp 559-572.

Popov,S.M., 1965: Some statistical characteristics of vertical structure of temperature and humidity fields, Izv.Atm. and Oceanic Pys. Ser.,Vol.1, No.1, pp 18-26, translated by C.M. Wade.

Preisendorfer,R.W., and T.P. Barnett, 1977: Significance tests for empirical orthogonal functions. Preprints Fifth Conference on Probability and Statistics in Atmospheric Sciences, Las Vegas, Amer. Meteor. Soc., 169-172.

Preisendorfer, R.W., F.W. Zwiers, and T.P. Barnett, 1981: Foundations of principal component selection rules. SIO Reference Series 81-4, Scripps Institute of Oceanography, LaJolla, Cal.

Rao, C.R., 1964: The use and interpretation of principal component analysis in applied research. Sankhya, Series A., Vol 26, 329-358.

Rayner, J.N., and D.A. Howarth, 1979: Antarctic Sea Ice: 1972-1975, The Geographical Review, Vol 69, No. 2, pp 202-223.

Rinne, J., and V. Karhila, 1979: Empirical orthogonal functions of 500 mb height in the northern hemisphere determined from a large sample. Quart. J.R. Met. Soc., Vol 105, 873-884.

Rinne, J., and S. Jarvenoja, 1979: Truncation of the EOF series representing the 500 mb height. Quart.J.R.Met.Soc., Vol 105, 885-897.

Rukhovets, L.V., 1963: The optimum representation of the vertical distribution of certain meteorological elements,Izv.Acad.Sci., USSR, Geophys.Ser., No. 4, pp 626-636, translated by J.S. Sweet.

Sellers,W.D., 1968: Climatology of monthly precipitation patterns in the western United States,1931-1966. Mon Wea Rev,96,No 1, 585-595.

Sellers,W.D., and D.N.Yarger,1969:The statistical prediction of the vertical ozone distribution. J.Appl. Met., Vol 8, p 357.

Smith,W.L.,H.M.Woolf, and H.E. Fleming, 1972:Retrieval of atmospheric temperature profiles from satellite measurements for dynamical forecasting, J.App. Met.

Smith,W.L.,and H.M.Woolf,1976:The use of eigenvectors of statistical covariance matrices for interpreting satellite sounding radiometer observations, Journal of the Atmospheric Sciences, Vol 33, No. 7 pp1117-1140

Spurrell, D.J., 1963: Some metallurgical applications of principal components, App. Statist., 12, p 180.

Steyaert, L.T., S. K. LeDuc and J. D. McQuigg, 1978: Atmospheric pressure and wheat yield modeling. Agric. Meteor., 19, 23-34.

Trenberth, K.E., 1975: A quasi-biennial standing wave in the Southern Hemisphere and interrelations with sea surface temperature. Quart. J. Roy. Meteor. Soc., 101, 55-74.

Vanicek, P., 1969: Astrophysics and Space Science 4, p 387.

Vanicek, P., 1971: Further development and properties of the spectral analysis by least squares, Astrophysics and Space Science 12, pp 10-73.

Walsh, J.E., and C.M. Johnson, 1979: Interannual atmospheric variability and associated fluctuations in arctic sea ice extent. J. Geophys. Res., 84, 6915-6928.

Walsh, J.E., and C.M. Johnson, 1979: An analysis of Arctic sea ice fluctuations, 1953-77. Journal of Phy. Oceanog., Vol 91, pp 580-591.

Wark, D.Q., and H.E. Fleming, 1966: Indirect measurements of atmospheric temperature profiles from satellites. Mon Wea Rev, Vol 94, No. 6, pp 351-362.

Weare, B.C., A.R. Navato, R.E. Newell, 1976: Empirical orthogonal analysis of Pacific sea surface temperatures. J. Phys. Ocean., Vol 6, pp 671-678.

Weare, B.C., 1979: A statistical study of the relationships between ocean surface temperatures and the Indian monsoon. J. of Atm. Sci., Vol 36, No 12, pp 2279-2291.

Weare, B.C., 1982: El Nino and tropical pacific ocean surface temperatures, J. of Phy. Ocean., Vol 12, pp 17-27.

Wells, E.E., and P. Vanicek, 1978: Least squares spectral analysis, Bedford Institute of Oceanography, Dartmouth/Nova Scotia/Canada, Report Series/ BI-R-78-8.

Wilheit, T.T., 1972: The electrically scanning microwave radiometer (ESMR) experiment, The Nimbus-5 User"s Guide, NASA Goddard Space Flight Center, pp 59-105.

Wilheit, T.T., W. Nordberg, J. Blinn, W. Campbell, and A. Edgerton, 1972: Aircraft measurements of microwave emission from Arctic sea ice, Remote Sensing of the Environment, Vol. 2, p 129.

Wilheit, T.T. et. al., 1975: A satellite technique for quantitatively mapping rainfall rates over the oceans. By T.T. Wilheit, M.S.V. Rao, T.C. Chang, E.B. Rogers, and J.S. Theon, J. Appl. Meteor., Vol 16, No. 5, pp 551-560.

Yakovleva, N.I., I.E. Chuvashina, and G.D. Kudashkin, 1968: Refinement of natural orthogonal functions of the pressure field (geopotential) over the northern hemisphere, Transactions of GGO, Leningrad, 201, pp 60-71.

Zwally, H.J., T.T. Wilheit, P. Gloersen, J.L. Mueller, 1976: Characteristics of Antarctic sea ice as determined by satellite-borne microwave images, COSPAR 19th Plenary MTG., Phila., Pa.

Zwally, H.J., and P. Gloersen, 1977: Passive microwave images of the polar regions and research applications, Polar Record, Vol. 18, No. 116, pp 431-450, printed in Great Britain.

Zwally, H.J., J.C. Comiso, and C.L. Parkinson, 1981: Satellite-derived ice data sets No. 1 Antarctic monthly average microwave brightness temperatures and sea ice concentrations 1973-1976, NASA TM 83812, Goddard Space Flight Center, Greenbelt, Md. 20771.

Zwally, H.J., J.C. Comiso, C.L. Parkinson, W.J. Campbell, F.D. Carsey, and P. Gloersen, 1983: Antarctic sea ice, 1973-1976; Satellite microwave observations, NASA SP 459, 45.

APPENDIX A

GEOMETRICAL INTERPRETATION OF PRINCIPAL COMPONENTS [1]

Principal components can be viewed geometrically as the projection of q points in a p-dimensional Euclidean space onto k orthogonal vectors of a "best fitting" k-dimensional subspace ($k \leq p$). Equivalently, they are linear functions of q measurements on p variables which possess certain optimal properties. The subspace is "best fitting" (Pearson 1901) in the sense that the sum of squares of the perpendicular distances from the points to the subspace is a minimum. The motivation for projecting the points onto a subspace of lower dimension is to represent the q measurements by less than p linear functions in such a way that there is a minimal loss of information content. The minimization procedure is equivalent to determining k orthogonal axes or directions such that there is maximum dispersion along the first principal axis, a second largest dispersion along the second principal axis, etc. The dispersion is a minimum along the kth principal axis (the dispersion is a measure of the variability and is the sum of squares of the perpendicular distances of the points to a line passing through the center of gravity of the points). The solution to the problem of finding a "best fitting" subspace to a scatter of points in a higher dimensional space involves the eigenvalues and eigenvectors of a matrix and was first investigated by Pearson (1901) and Frisch (1929).

As a simple example, consider the scatter of points in Figure A-1. The "best fitting" one-dimensional subspace passing through the center of gravity C of the 7 two-dimensional points is the line L_{PC} (obtained by minimizing the sum of squares of the perpendiculars from the points to the line). The "standard" least squares straight

---

(1) The development here follows that of Rao (1964) who gives an excellent treatment on the use and interpretation of principal components in applied research and who discusses many of their optimal properties. Kshsirsagar (1972) is also an excellent reference on the subject and the proof of one of the optimal properties found in this appendix is due to him. The appendix is self-contained.

line fit to these points is the line L_{LS} (obtained by minimizing the sum of squares of the vertical distances from the points to the line). Note that the dispersion of the points is a maximum in the direction of L_{PC} (i.e., the second moment about a line passing through the center of gravity is the greatest in this particular direction). The second principal axis (not shown) is orthogonal to L_{PC} and is in the direction of L_{LS}, also passing through C.

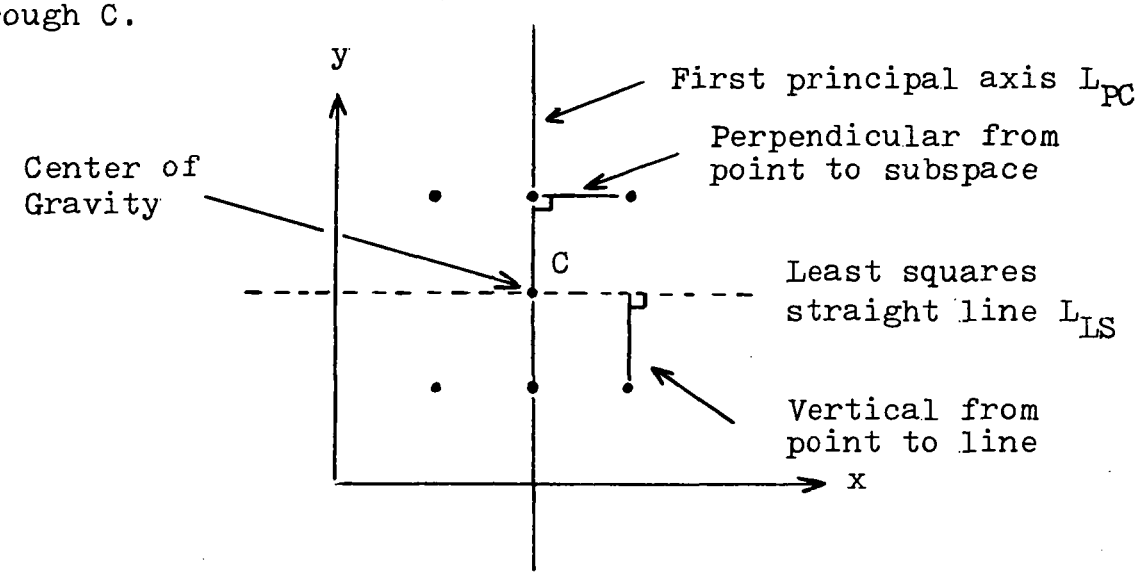

Figure A-1

We can represent q points in a p-dimensional Euclidean space by the matrix X

$$X = \begin{pmatrix} x_{11} & \cdots & x_{1q} \\ \cdots & & \\ x_{p1} & \cdots & x_{pq} \end{pmatrix} = (x_1, \ldots, x_q) = (x_{ij}) \qquad (A.1)$$

where the jth point, x_j, is the jth column of X.

The center of gravity of the q points is $\bar{x}$ where the ith coordinate is

$$\bar{x}_i = (1/q) \sum_{j=1}^{q} x_{ij} \qquad (A.2)$$

$$(i = 1,2,\ldots,p)$$

The points measured from their center of gravity, $v_{ij} = (x_{ij} - \bar{x}_i)$ $(i = 1,2,\ldots,p;\ j = 1,2,\ldots,q)$ can be written

$$V = \begin{pmatrix} v_{11} & \cdots & v_{1q} \\ \cdots & & \\ v_{p1} & \cdots & v_{pq} \end{pmatrix} = (v_1,\ldots,v_q) = (v_{ij}) \qquad (A.3)$$

The total dispersion (or scatter) matrix S is

$$S = VV' = (s_{ij}) \qquad (A.4)$$

and is positive semi-definite with p eigenvalues $d_1 \geq d_2 \geq \ldots \geq d_p \geq 0$ which are the roots of

$$\left|S - dI_p\right| = 0 \qquad (A.5)$$

Corresponding to each d_j there is an orthonormal eigenvector e_j which satisfies

$$Se_j = d_j e_j \qquad (A.6)$$

or in matrix notation

$$E'SE = D = \operatorname{diag}(d_1 \ldots d_p) \qquad (A.7)$$

where

$$E = (e_1 \ldots e_p) \qquad (A.8)$$

$$EE' = E'E = I_p \qquad (A.9)$$

and I_p is the identity matrix of order p.

Equation (A.7) can be written

$$S = d_1 e_1 e_1' + \ldots + d_p e_p e_p' \tag{A.10}$$

$$I_p = e_1 e_1' + \ldots + e_p e_p' \tag{A.11}$$

The representation of S and I_p in (A.10) and (A.11) is known as the spectral decomposition of the matrix S and I_p respectively (Good 1969 and Appendix B).

By definition a k-dimensional subspace is specified by a point (or origin) and k orthogonal vectors. As previously mentioned Pearson defined a "best fitting" subspace as one in which the sum of squares of the perpendicular distances from the points to the subspace is a minimum. Such a subspace passes through the center of gravity of the points.

Let $h_1, h_2, \ldots, h_k$ be k orthogonal vectors which together with $\bar{x}$ specify the k-dimensional subspace. Without loss of generality we may assume the h_i are orthonormal vectors. The square of the perpendicular distance from the ith point to the subspace is then

$$l_i^2 = (x_i-\bar{x})'(x_i-\bar{x}) - \left(\left[h_1'(x_i-\bar{x})\right]^2 + \ldots + \left[h_k'(x_i-\bar{x})\right]^2 \right) \tag{A.12}$$

Summing (A.12) over all q points we obtain

$$Q = \sum_{i=1}^{q} l_i^2 = \sum_{i=1}^{p} s_{ii} - \sum_{i=1}^{k} h_i' S h_i$$

$$= \text{trace}(S) - \text{trace}(H'SH) \tag{A.13}$$

where

$$H = (h_1 \ldots h_k) = (h_{ij}) \tag{A.14}$$

$$H'H = I_k \tag{A.15}$$

Since the eigenvectors e_j are orthogonal they are linearly independent and form a basis for the p-dimensional space. Therefore we can write h_i as a linear function of the e_j

$$h_i = c_{i1}e_1 + \ldots + c_{ip}e_p \qquad (i = 1,2,\ldots,k) \tag{A.16}$$

or in matrix notation

$$H = EC' \tag{A.17}$$

where E is given by (A.8) and

$$C = \begin{pmatrix} c_{11} & \cdots & c_{1p} \\ & & \\ c_{k1} & \cdots & c_{kp} \end{pmatrix} \tag{A.18}$$

with

$$CC' = I_k \tag{A.19}$$

Using (A.7), (A.9), and (A.17) trace(H'SH) becomes

$$\text{trace}(H'SH) = \text{trace}(CDC')$$

$$= d_1(c_{11}^2 + \ldots + c_{k1}^2) + \ldots + d_p(c_{1p}^2 + \ldots + c_{kp}^2) \qquad (A.20)$$

where each of the coefficients of d_i is ≤ 1 and the sum of all the coefficients is k by (A.19).

In order to maximize trace(H'SH) the optimum choice for the coefficients is unity for $d_1,\ldots,d_k$ and zero for the others. This means $c_{ii} = 1$ for $i = 1,2,\ldots,k$, $c_{ij} = 0$ for all other i and j which is possible by choosing $h_i = e_i$ for $i = 1,2,\ldots,k$.

Therefore

$$\max_{c_{ij}} \text{trace}(CDC') = d_1 + \ldots + d_k \qquad (A.21)$$

and the minimum of Q in (A.13) is

$$\min_{h_i} Q = d_{k+1} + \ldots + d_p \qquad (A.22)$$

which is attained when $h_i = e_i$ $(i = 1,2,\ldots,k)$.

The actual representation of points in the "best fitting" lower dimensional subspace is, letting $E_k = (e_1,\ldots,e_k)$

$$E_k'X = \begin{pmatrix} e_1'x_1 & \cdots & e_1'x_q \\ \cdots & & \\ e_k'x_1 & \cdots & e_k'x_q \end{pmatrix} \qquad (A.23)$$

The first row of $E_k'X$ gives the best one-dimensional representation of the points; the first two rows give the best two-dimensional representation, etc.

In similar manner

$$Y = E_k'V = \begin{pmatrix} e_1'v_1 & \cdots & e_1'v_q \\ \cdots & & \\ e_k'v_1 & \cdots & e_k'v_q \end{pmatrix} = \begin{pmatrix} y_1 \\ \vdots \\ y_k \end{pmatrix} = (y_{ij}) \qquad (A.24)$$

gives the best fitting lower dimensional representation of the deviations of the points from their center of gravity. Here y_i ($i = 1,2,\ldots,k$) is the i<u>th</u> principal component as used in the text.

Another optimal property of the first k eigenvectors of S should be noted.

In the sense of least squares the <u>sum of the first k terms</u> in the spectral decomposition (or singular value decomposition) of S gives the <u>best matrix of rank k that approximates S</u>.

Thus, if B is any matrix of rank k then

$$\min_B \|S - B\| = (d_{k+1}^2 + \ldots + d_p^2)^{\frac{1}{2}} \qquad (A.25)$$

where the Euclidean norm of A, $\|A\|$, is

$$\|A\| = \left(\sum_{i,j} a_{ij}^2 \right)^{\frac{1}{2}} \qquad (A.26)$$

See Appendix B.

APPENDIX B

RELATIONSHIP BETWEEN SINGULAR DECOMPOSITION AND EOF/PRINCIPAL COMPONENT ANALYSIS

Let V be a real (p x q) data matrix of rank r. Using the singular decomposition theorem (Good 1969) we can write

$$V = e_1 d_1^{\frac{1}{2}} f_1' + \ldots + e_r d_r^{\frac{1}{2}} f_r' \tag{B.1}$$

where the column vectors e_j and f_j are respectively the left singular vectors of V (or eigenvectors of VV') and the right singular vectors of V (or eigenvectors of V'V), and the $d_j^{\frac{1}{2}}$ are the singular values of V or the square roots of the positive eigenvalues of VV' (or of V'V) with

$$d_1^{\frac{1}{2}} \geq d_2^{\frac{1}{2}} \geq \ldots \geq d_r^{\frac{1}{2}} > 0 \tag{B.2}$$

and

$$e_i' e_j = f_i' f_j = \delta_{ij} \tag{B.3}$$

If p is the number of spatial points and q the number of time points and the row means (time averages) have been removed from the data array V, then the e_j are sometimes referred to as spatial EOF's (empirical orthogonal functions) and the f_j as time EOF's (Lorenz 1956).

Using (B.1) and the orthonormal property of e_j and f_j in (B.3) we can write

$$V' = f_1 d_1^{\frac{1}{2}} e_1' + \ldots + f_r d_r^{\frac{1}{2}} e_r' \tag{B.4}$$

$$VV' = e_1 d_1 e_1' + \ldots + e_r d_r e_r' \tag{B.5}$$

$$V'V = f_1 d_1 f_1' + \ldots + f_r d_r f_r' \tag{B.6}$$

To show that e_j is an eigenvector of VV' corresponding to d_j

we use (B.3) and (B.5)

$$(VV')e_j = d_j e_j \tag{B.7}$$

To show that f_j is an eigenvector of $V'V$ corresponding to d_j we use (B.3) and (B.6)

$$(V'V)f_j = d_j f_j \tag{B.8}$$

Define the principal component y_j corresponding to e_j as

$$y_j = e_j'V \tag{B.9}$$

Then using (B.1) and (B.3) y_j becomes

$$y_j = d_j^{\frac{1}{2}} f_j' \tag{B.10}$$

and we see that y_j' is also an eigenvector of $V'V$ corresponding to d_j (not normalized).

In similar manner define the principal component z_j corresponding to f_j as

$$z_j = f_j'V' \tag{B.11}$$

Then using (B.3) and (B.4) z_j becomes

$$z_j = d_j^{\frac{1}{2}} e_j' \tag{B.12}$$

and we see that z_j' is also an eigenvector of VV' corresponding to d_j (not normalized).

Using (B.3), (B.10), and (B.12) we can write

$$y_i y_j' = z_i z_j' = d_i \delta_{ij} \tag{B.13}$$

and we see that the y_j and z_j row vectors are also orthogonal.

Using (B.10) and (B.12) in (B.1), (B.4), (B.5), and (B.6) we can write the singular decomposition of these matrices in terms of the eigenvectors of VV' and $V'V$ and their principal components.

$$V = e_1 y_1 + \ldots + e_r y_r \tag{B.14}$$

$$V' = f_1 z_1 + \ldots + f_r z_r \tag{B.15}$$

$$VV' = z_1' z_1 + \ldots + z_r' z_r \tag{B.16}$$

$$V'V = y_1' y_1 + \ldots + y_r' y_r \tag{B.17}$$

The trace of VV' (or of $V'V$) is

$$\begin{aligned} \text{Trace}(VV') &= \text{Trace}(y_1' y_1) + \ldots + \text{Trace}(y_r' y_r) \\ &= \|y_1\|^2 + \ldots + \|y_r\|^2 \\ &= y_1 y_1' + \ldots + y_r y_r' \\ &= d_1 + d_2 + \ldots + d_r \end{aligned} \tag{B.18}$$

where $\|x\|$ is the Euclidean norm of x.

We can use the first $k \leq r$ terms in the singular decomposition of the matrices in (B.1), (B.4), (B.5), and (B.6) to approximate them. Thus, for V we have the approximation $\bar{V}$

$$V \doteq \bar{V} = e_1 d_1^{\frac{1}{2}} f_1' + \ldots + e_k d_k^{\frac{1}{2}} f_k'$$

$$= e_1 y_1 + \ldots + e_k y_k \qquad \text{(B.19)}$$

In the sense of least squares $\bar{V}$ gives the best matrix of rank k that approximates V. That is, $(V - \bar{V})$ has minimum norm. In order to see this, since the pq matrices $e_i f_j'$ $(i = 1,2,\ldots,p;$ $j = 1,2,\ldots,q)$ form a basis for the vector space of (p x q) matrices, we can write an arbitrary approximation for V with rank k, or V_a, as

$$V_a = \sum_{i,j} \alpha_{ij} e_i f_j' \qquad \text{(B.20)}$$

Writing the <u>complete singular decomposition of V</u> (Good 1969) as

$$V = \sum_{i,j} d_i^{\frac{1}{2}} \delta_{ij} e_i f_j' \qquad \text{(B.21)}$$

we have

$$\|V - V_a\|^2 = \sum_{i,j=1}^{r} (d_i^{\frac{1}{2}} \delta_{ij} - \alpha_{ij})^2 \qquad \text{(B.22)}$$

and the optimum choice for α_{ij} is

$$\alpha_{ij} = d_i^{\frac{1}{2}} \delta_{ij} \qquad \text{(B.23)}$$

$$(i = 1,2,\ldots,k)$$

This gives $V_a = \bar{V}$ as the best matrix of rank k which approximates V. The minimum attained is

$$\|V - \bar{V}\|^2 = d_{k+1} + \ldots + d_r \qquad (B.24)$$

Since the sum of all the d_j $(j = 1,2,\ldots,r)$ is the trace T of VV', each term in the expansion of V, e.g., the jth explains

$$\left[d_j/(d_1 + \ldots + d_r)\right] x\ 100\%$$

of T.

In similar fashion it can be shown that the first $k \leq r$ terms in the expansion of $S = VV'$ in (B.5) gives us the best matrix in the least squares sense which approximates S. That is, if B is any matrix of rank k then (S - B) has minimum norm and equation (A.25) in Appendix A holds.

The above illustrates the dual role of eigenvectors and principal components in the V and V' spaces. If e_j is an orthonormal eigenvector of VV' corresponding to the eigenvalue $d_j \neq 0$ with principal component $y_j = e_j'V$, then $f_j = d_j^{-\frac{1}{2}} y_j'$ is an orthonormal eigenvector of V'V. If f_j is an orthonormal eigenvector of V'V corresponding to $d_j \neq 0$ with principal component $z_j = f_j'V'$, then $e_j = d_j^{-\frac{1}{2}} z_j'$ is an orthonormal eigenvector of VV'.

APPENDIX C

RELATIONSHIP BETWEEN A PARTITIONED AND A NON-PARTITIONED MATRIX V (1)

Let V be an arbitrary real data matrix with dimension (p x q) and rank $r \leq q \leq p$. Then we can write (Appendix B)

$$\begin{aligned} V &= ED^{\frac{1}{2}}F' = EY \\ &= e_1 d_1^{\frac{1}{2}} f_1' + \ldots + e_r d_r^{\frac{1}{2}} f_r' \\ &= e_1 y_1 + \ldots + e_r y_r \end{aligned} \qquad (C.1)$$

with

$$E'E = F'F = I_r$$

$$E = (e_1 \ldots e_r)$$

$$F = (f_1 \ldots f_r)$$

$$D^{\frac{1}{2}} = \mathrm{diag}(d_1^{\frac{1}{2}} \ldots d_r^{\frac{1}{2}})$$

$$YY' = D = \mathrm{diag}(d_1 \ldots d_r)$$

where the e_j and f_j ($j = 1,2,\ldots,r$) are respectively the left and right singular vectors of V and the $d_j^{\frac{1}{2}}$ are the singular values of V,

$$d_1^{\frac{1}{2}} \geq d_2^{\frac{1}{2}} \geq \ldots \geq d_r^{\frac{1}{2}} > 0$$

Since the rank of V is r

$$d_{r+1}^{\frac{1}{2}} = \ldots = d_q^{\frac{1}{2}} = 0$$

Partition V into M matrices V_i with dimension $(p_i \times q)$ and rank $r_i \leq q$ where $p_1 + \ldots + p_M = p$, $r_1 + \ldots + r \geq r$, and use the singular value decomposition for each V_i ($i = 1,2,\ldots,M$)

$$V = \begin{pmatrix} V_1 \\ \vdots \\ V_M \end{pmatrix} = \overline{EY}$$

$$= \bar{e}_1\bar{y}_1 + \ldots + \bar{e}_{\bar{r}}\bar{y}_{\bar{r}} \qquad (C.2)$$

where $\bar{r} = r_1 + \ldots + r_M$ and

$$V_i = E_i D_i^{\frac{1}{2}} F_i' = E_i Y_i$$

$$= {}_ie_1({}_iy_1) + \ldots + {}_ie_{r_i}({}_iy_{r_i})$$

$$(i = 1,2,\ldots, M)$$

$$\bar{E} = \begin{pmatrix} E_1 & & \\ & \ddots & \\ & & E_M \end{pmatrix}$$

$$\bar{Y} = \begin{pmatrix} Y_1 \\ \vdots \\ Y_M \end{pmatrix}$$

The $\bar{e}_j$ vectors (columns of $\bar{E}$) form an orthogonal set. Let $\bar{p}_i = \bar{p}_{i-1} + p_i$, $\bar{p}_o = 0$, and $\bar{r}_i = \bar{r}_{i-1} + r_i$, $\bar{r}_o = 0$. Then we can write

$$\bar{e}_{k,\bar{r}_{i-1}+j} = \begin{cases} {}_ie_{kj} & \text{for } 1 \leq j \leq r_i \text{ and} \\ & \bar{p}_{i-1} < k \leq \bar{p}_i \\ & 1 \leq i \leq M \\ 0 \text{ otherwise} \end{cases}$$

where ${}_ie_{kj}$ is the kth element of ${}_ie_j$ and the column vectors ${}_ie_j$ of E_i are the eigenvectors from the ith subdivision.

Using the orthonormal property of the ${}_ie_j$ vectors

$$\bar{e}_i'\bar{e}_j = \delta_{ij}$$

The $\bar{y}_j$ vectors (rows of $\bar{Y}$) are related to the ${}_iy_j$ (principal components corresponding to the ${}_ie_j$ or row vectors of Y_i)

$$\bar{y}_{\bar{r}_{i-1}+j} = {}_iy_j \qquad \begin{matrix} (1 \leq j \leq r_i) \\ (1 \leq i \leq M) \end{matrix}$$

It should be noted that the $\bar{y}_j$ vectors do not form an orthogonal set. They can, however, be orthogonalized. That is, using the singular value decomposition for $\bar{Y}$, V in (C.2) becomes [2]

$$V = \bar{E}\bar{Y} = \bar{E}(A\bar{D}^{\frac{1}{2}}H') = G\bar{D}^{\frac{1}{2}}H'$$

$$= GW = g_1w_1 + \ldots + g_sw_s \qquad (C.3)$$

The rank of each of the matrices G, $\bar{D}^{\frac{1}{2}}$, and H is s where $s \leq \bar{r}$. Therefore $\bar{D}^{\frac{1}{2}}$ has s positive elements along its diagonal

and

$$\bar{D}^{\frac{1}{2}} = G'VH \qquad (C.4)$$

since $H'H = G'G = I_s$.

Since the rank of the product of matrices is less than or equal to the rank of any of the individual factors, from (C.3) $r \leq s$ and from (C.4) $s \leq r$. Therefore $s = r$.

Letting $S = VV'$ we see from (C.1) and (C.3) that there are two semi-orthogonal matrices E and G which diagonalize S.

$$E'SE = YY' = D \qquad (C.5)$$

$$G'SG = WW' = \bar{D} \qquad (C.6)$$

Since the characteristic equation is the same in both cases and the eigenvalues have been ordered (largest to smallest) D and $\bar{D}$ must be identical. Let D be the matrix.

We must show now that the eigenvectors e_j and g_j are identical up to a sign change in their components.

Let e_j and g_j be two eigenvectors which correspond to d_j with

$$e_j' = (e_{1j}, \ldots, e_{pj})$$

$$g_j' = (g_{1j}, \ldots, g_{pj})$$

Then from (C.5) and (C.6)

$$e_j'Se_j = g_j'Sg_j = d_j$$

which can be written as

$$\sum_{i,k} e_{kj} e_{ij} s_{ik} = \sum_{i,k} g_{kj} g_{ij} s_{ik}$$

from which by equating like coefficients of the elements of S, i.e., s_{ik}, we obtain

$$e_{ij}^2 = g_{ij}^2 \qquad (k = i) \tag{C.7}$$

$$e_{kj} e_{ij} = g_{kj} g_{ij} \qquad (k \neq i) \tag{C.8}$$

Equation (C.7) has two solutions

$$e_{ij} = \pm g_{ij} \quad (k = i) \tag{C.9}$$

Substituting (C.9) into (C.8) gives

$$e_{kj} = \pm g_{kj} \quad (k \neq i)$$

and therefore the eigenvectors e_j and g_j are identical up to a sign change in their components.

The trace T of S can be written in terms of the trace T_i of $S_i = V_i V_i'$ $(i = 1,2,\ldots,M)$

$$T = \|V\|^2 = \sum_{j=1}^{r} d_j = \sum_{i=1}^{M} \|V_i\|^2$$

$$= \sum_{i=1}^{M} \left(\sum_{j=1}^{r_i} d_j \right) = T_1 + \ldots + T_M \tag{C.10}$$

$$(r_1 + \ldots + r_M \triangleq r)$$

where the d_j ($j = 1,2,\ldots,r$) are the positive eigenvalues of S, the ${}_id_j$ ($j = 1,2,\ldots,r_i$) are the positive eigenvalues of S_i or elements of D_i, and $\|A\|$ is the Euclidean norm of $A = (a_{ij})$, $\|A\|^2 = \sum_{i,j} a_{ij}^2$.

It should be noted that if $i_1, i_2, \ldots, i_M$ is an arbitrary ordering of the integers from 1 to M, then there exists a (p x p) permutation matrix P such that PV will order the $V_1, \ldots, V_M$ in the order $V_{i_1}, \ldots, V_{i_M}$ and the trace remains invariant. That is,

$$\text{trace } (PV)(PV)' = \text{trace } (PV)'(PV)$$

$$= \text{trace } (V'P'PV) = \text{trace } (V'V) = T \qquad \text{(C.11)}$$

Let us approximate V by selecting only k_i eigenvectors (and corresponding principal components) from each subdivision such that $100\alpha\%$ of the trace T is accounted for where $0 \leq \alpha \leq 1$. That is, let $k_i \leq r_i$ be the smallest integer such that

$$\sum_{j=1}^{k_i} {}_id_j \geq \alpha T_i \qquad \text{(C.12)}$$

Then, using the first k_i terms in the singular decomposition of each V_i, i.e., $\bar{V}_i$ (see Appendix B) V is approximated by $\hat{V}$ ($\hat{k} = k_1 + \ldots + k_M$)

$$V \doteq \hat{V} = \begin{pmatrix} \bar{V}_1 \\ \vdots \\ \bar{V}_M \end{pmatrix} = g_1 w_1 + \ldots + g_{\hat{k}} w_{\hat{k}} \qquad \text{(C.13)}$$

The g and w vectors in (C.13) are the eigenvectors and components of $\hat{V}\hat{V}'$. In (C.3) they are the eigenvectors and components of VV'. If $k_i = r_i$ ($i = 1,2,\ldots,M$), $\hat{V} = V$ and they then refer to the same matrix.

Using (C.10) and (C.12)

$$\sum_{i=1}^{M}\left(\sum_{j=1}^{k_i} d_j\right) \geq \sum_{i=1}^{M} \alpha T_i = \alpha T \qquad (C.14)$$

Now let $\bar{k} \leq \hat{k}$ be the smallest integer such that

$$\sum_{j=1}^{\bar{k}} \bar{d}_j \geq \alpha T$$

where $\bar{d}_j = w_j w_j'$ are the positive eigenvalues of $\bar{Y}\bar{Y}'$, $\bar{d}_1 \geq \bar{d}_2 \geq \ldots \geq \bar{d}_{\bar{k}} \geq \bar{d}_{\hat{k}} > 0$ and k_i ($i = 1,2,\ldots,M$) principal components from Y_i have been concatenated to form $\bar{Y}$.

The matrix $\hat{V}$ is then approximated by $\bar{V}$

$$\hat{V} \doteq \bar{V} = g_1 w_1 + \ldots + g_{\bar{k}} w_{\bar{k}} \qquad (C.15)$$

with

$$\hat{T} = \|\hat{V}\|^2 = \sum_{j=1}^{\hat{k}} \bar{d}_j \geq \sum_{j=1}^{\bar{k}} \bar{d}_j = \bar{T} \geq \alpha T \qquad (C.16)$$

where $\hat{T}$ is the trace of $\bar{Y}\bar{Y}'$ and $\bar{T}$ the trace of $\bar{V}\bar{V}'$

It should be noted that we have used $\bar{V}$ here as the best matrix in the least squares sense of rank $\bar{k}$ which approximates $\hat{V}$, whereas in Appendix B, $\bar{V}$ was defined as the best matrix of rank k approximating V. If $k_i = r_i$ for $i = 1,2,\ldots,M$, then $V = \hat{V}$, $\hat{k} = r$, $\bar{k} = k$ and the two definitions are consistent. In Appendix D for the first partitioning level ($l = 1$) we set $\hat{V}_{(1)} = V$ and then $\bar{V}$ is the least squares approximation to both $\hat{V}_{(1)}$ and V which is again consistent with Appendix B and this appendix.

(1) The partitioning and joining scheme described in this appendix was first presented by Yakovleva et. al (1968) and is documented in Rinne and Karhila (1979). The difference between the presentation given here and that of Yakovleva is that the number of eigenvectors and principal components to be joined at the various levels is variable and depends upon the required tolerance level α and the magnitudes of the largest eigenvalues within each subdivision. In the cited references a fixed number of vectors and components are joined together.

(2) The a_j vectors (columns of $\underline{A}$) or left singular vectors of $\overline{Y}$ (also the eigenvectors of $\overline{Y}\overline{Y}$) are the "joining vectors" which are equivalent to the "joining functions" in Yakovleva.

APPENDIX D

PARTITIONING AND JOINING IN GENERAL

Let V be a real (p x q) data matrix ($q \leq p$) with rank r where the row means have been subtracted from the data. Partition V into M subarrays V_i with dimension (p_i x q) and rank r_i where $p_1 + \ldots + p_M = p$, $r_1 + \ldots + r_M \geq r$, $r_i \leq q$ and $r \leq q$

$$V = \begin{pmatrix} V_1 \\ \vdots \\ V_M \end{pmatrix} \tag{D.1}$$

From Appendix C if P is any (p x p) permutation matrix which reorders the V_i

$$PV = \begin{pmatrix} V_{i_1} \\ \vdots \\ V_{i_M} \end{pmatrix} \tag{D.2}$$

where i_j (j = 1,2,...,M) are the integers i (i = 1,2,...,M) in some order, then the trace remains unchanged. That is

$$T = \|V\|^2 = \|PV\|^2 = T_{i_1} + ,.. + T_{i_M} \tag{D.3}$$

with T the trace of VV', T_i the trace of $V_i V_i'$, and $\|A\|$ the Euclidean norm of $A = (a_{ij})$, $\|A\|^2 = \sum_{i,j} a_{i,j}^2$.

Sets of local EOF's corresponding to the various subdivisions of the data array, V_i, may be ordered and joined in a number of ways.

The ordering of the M matrices in (D.2) is only 1 out of a possible M! such permutations. For each permutation the V_i can be joined together in 2^{M-1} possible combinations giving a total of $M!2^{M-1}$ possible arrangements. In each case we are interested in retaining $100\alpha\,\%$ of the total information content in the data (i.e., $100\alpha\,\%$ of the trace T) where α is a selected tolerance level ($0 \leq \alpha \leq 1$).

In general let there be L partitioning levels with M_l matrices and N_l groups of matrices at the lth level ($l = 1,2,\ldots,L$), and ${}_l m_n$ matrices in the nth group which we will concatenate and join together (Appendix C), ${}_l m_1 + \ldots + {}_l m_{N_l} = M_l$.

The partitioning and joining procedure can now be described by the following matrices at the lth level

$$P_l \bar{V}_{(l)} = \bar{\bar{V}}_{(l)} = \hat{V}_{(l+1)} \triangleq \bar{V}_{(l+1)} \qquad (D.4)$$

$$(l = 1,2,\ldots,L)$$

where

$$\bar{V}_{(l)} = \begin{pmatrix} \bar{V}_1 \\ \vdots \\ \bar{V}_{M_l} \end{pmatrix} \qquad (D.5)$$

$$\bar{\bar{V}}_{(l)} = \begin{pmatrix} \bar{V}_{l_1} \\ \vdots \\ \bar{V}_{l_{M_l}} \end{pmatrix} \qquad (D.6)$$

$$\hat{\bar{V}}_{(l+1)} = \begin{pmatrix} \hat{\bar{V}}_1 \\ \vdots \\ \hat{\bar{V}}_{N_l} \end{pmatrix} \qquad (D.7)$$

The $\bar{V}_i$ (elements of $\bar{V}_{(l)}$) are least squares approximations to the $\hat{V}_i$ ($i=1,2,\ldots,M_l$) and consist of the first k_i terms in the singular decomposition of $\hat{V}_i$ (see Appendix C). P_l is a permutation matrix. Initially, $M_l = M$, $P_l = I_M$, $\hat{V}_{(2)} = \bar{V}_{(1)} = V$, $\hat{V}_i = \bar{V}_i = V_i$ for $i = 1,2,\ldots,M$.

The elements of $\bar{\bar{V}}_{(l)}$ are the permuted elements of $\bar{V}_{(l)}$ which are grouped into N_l groups, the nth group consisting of the following set of matrices

$$\text{nth group} = \left\{ \bar{V}_{l_j} \right\}_{j=\bar{m}_{n-1}+1}^{j=\bar{m}_n} \qquad (D.8)$$

$$(\bar{m}_n = \bar{m}_{n-1} + m_n,\ \bar{m}_o = 0)$$

$$(n = 1,2,\ldots, N_l)$$

where the l has been suppressed in ${}_l m_n$ and ${}_l \bar{m}_n$ for simplicity.

Joining the m_n matrices in (D.8) gives $\hat{\bar{V}}_n$, and element of $\hat{\bar{V}}_{(l+1)}$ ($n = 1,2,\ldots,N_l$). From Appendix C, $\hat{\bar{V}}_n$ can be written using the subscript n for joined matrices in the nth group

$$\hat{V}_n = \bar{E}_n \bar{Y}_n = \bar{E}_n (A_n \bar{D}_n^{\frac{1}{2}} H_n') = G_n \bar{D}_n^{\frac{1}{2}} H_n' = G_n W_n \qquad (D.9)$$

The A_n matrix consists of the joining vectors or functions which are also the left singular vectors of $\bar{Y}_n$ or equivalently the eigenvectors of $\bar{Y}_n \bar{Y}_n'$.

Each of the m_n elements of $\bar{E}_n$

$$\bar{E}_n = \begin{pmatrix} {}_nE_1 & & \\ & \ddots & \\ & & {}_nE_{m_n} \end{pmatrix} \qquad (D.10)$$

or the ${}_nE_i$ $(i = 1,2,\ldots,m_n)$ matrices consists of a set of k_i local EOF's (columns of ${}_nE_i$).

In similar fashion each of the m_n elements of $\bar{Y}_n$

$$\bar{Y}_n = \begin{pmatrix} {}_nY_1 \\ \vdots \\ {}_nY_{m_n} \end{pmatrix} \qquad (D.11)$$

or the ${}_nY_i$ principal component matrices consists of k_i principal components corresponding to the k_i EOF's in ${}_nE_i$.

The columns of G_n are the "global" EOF's for the nth group formed from the m_n sets of local EOF's.

Similar to Appendix C, for each $\hat{V}_n$, the first $\bar{k}$ terms in its singular decomposition become the $\bar{V}_n$ matrix in $\bar{V}_{(l+1)}$, and we set $k_n = \bar{k}$ and $M_{l+1} = N_l$ $(n = 1,2,\ldots,N_l)$.

From (D.4)

$$\bar{V}_{(L+1)} \doteq (P_1 \ldots P_l)V \tag{D.12}$$

and therefore

$$V \doteq (P^{-1} \ldots P_L^{-1})\bar{V}_{(L+1)} \tag{D.13}$$

Denote by $\bar{T}_{(l)}$ the trace of $\bar{V}_{(l)}\bar{V}'_{(l)}$. We can write

$$\bar{T}_{(l+1)} \geq \alpha^{\frac{1}{L}} \bar{T}_{(l)} \tag{D.14}$$

$$(l = 1,2,\ldots,L)$$

and then

$$\bar{T}_{(L+1)} \geq \alpha T \tag{D.15}$$

We therefore can approximate V at a $100\alpha\%$ level and each of the k_i is determined such that $k_i = \bar{k}$ where $\bar{k}$ is the smallest integer such that

$$\sum_{j=1}^{\bar{k}} \bar{d}_j \geq \alpha^{\frac{1}{L}} T_1$$

Table 1

First 10 Eigenvalues

Eigenvalue Number	Eigenvalue $(^{o}K)^{2}$	% Contribution To Variance	Cumulative Contribution (%)
1	7026087.28	68.78	68.78
2	855772.20	8.38	77.16
3	458117.91	4.48	81.64
4	320376.35	3.14	84.78
5	208065.12	2.04	86.82
6	142705.51	1.40	88.21
7	111005.21	1.09	89.30
8	100980.40	0.99	90.29
9	75789.78	0.74	91.03
10	61717.53	0.60	91.63

Total variance = 10215181 $(^{o}K)^{2}$

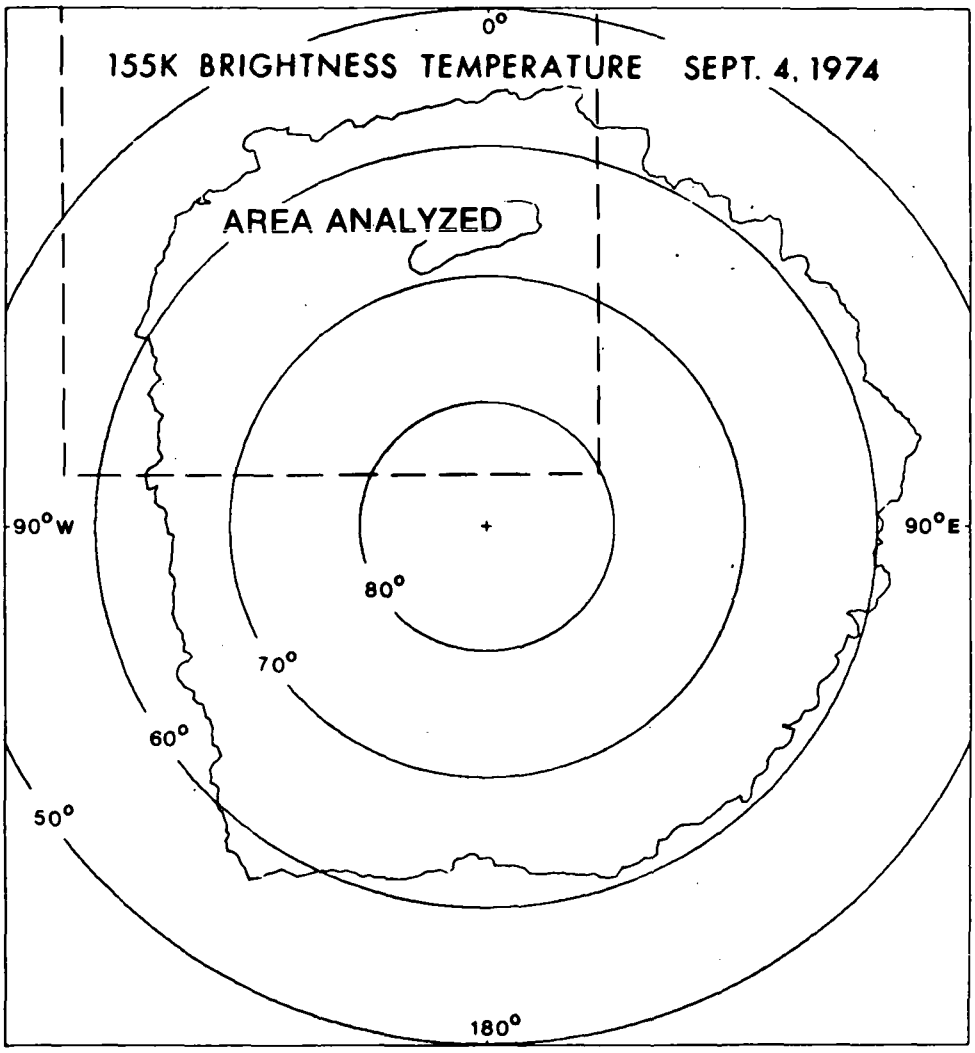

FIGURE 1: MAXIMUM ICE EXTENT AS REPRESENTED BY THE 155°K BRIGHTNESS ISOTHERM (FROM RAYNER AND HOWARTH) AND AREA ANALYZED

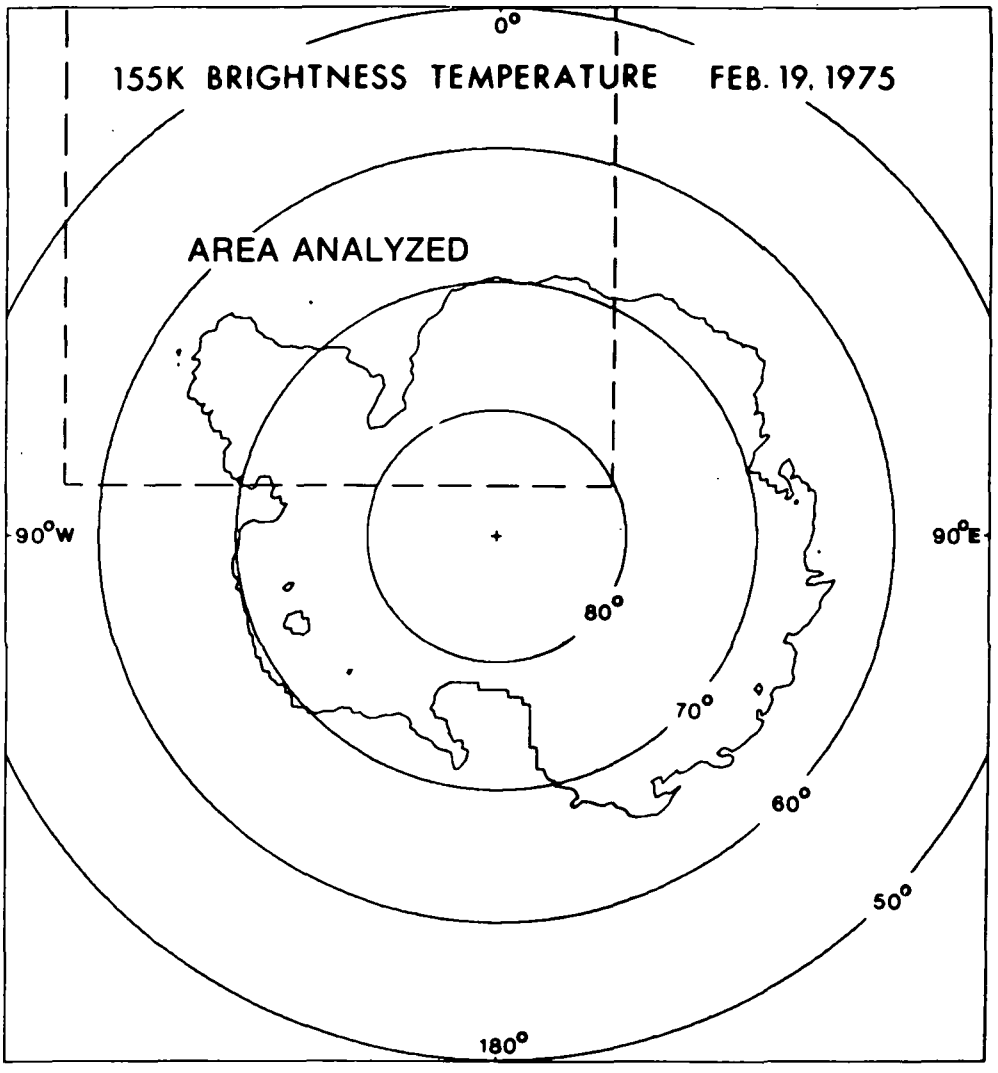

FIGURE 2: MINIMUM ICE EXTENT AS REPRESENTED BY THE 155°K BRIGHTNESS ISOTHERM (FROM RAYNER AND HOWARTH) AND AREA ANALYZED

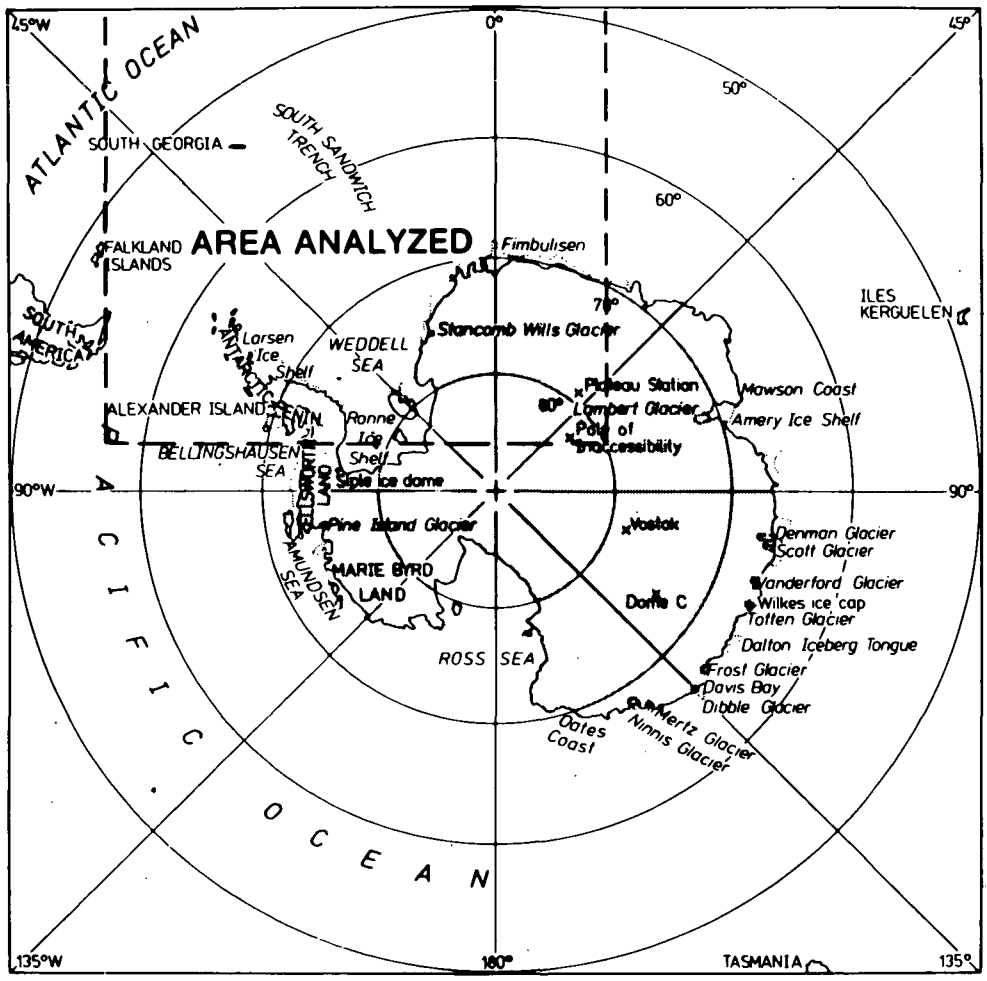

FIGURE 3: LOCATION MAP FOR SOUTH POLAR REGION (TAKEN FROM ZWALLY AND GLOERSEN 1977) SHOWING AREA ANALYZED

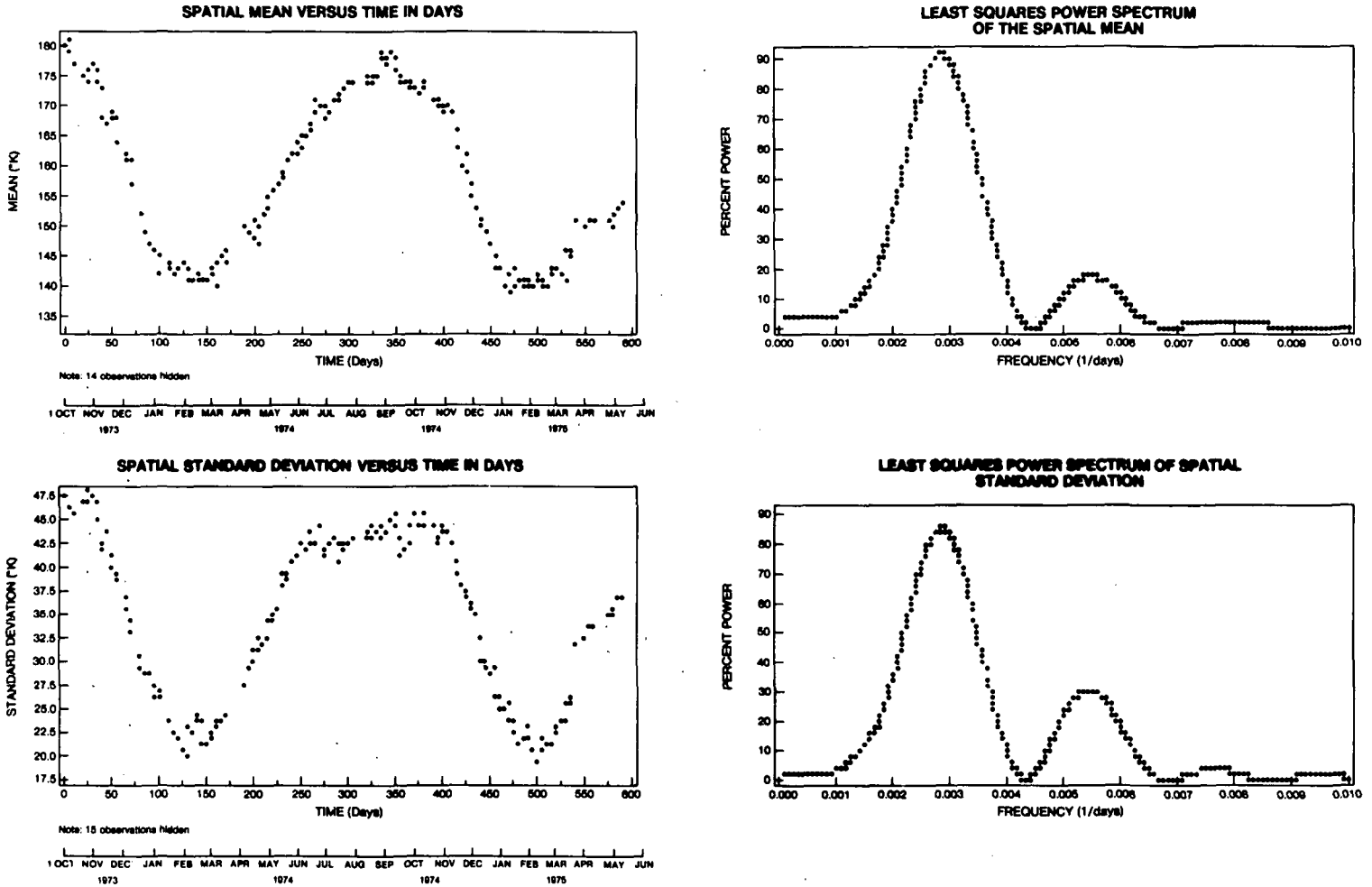

FIGURE 4: SPATIAL MEAN AND STANDARD DEVIATION VERSUS TIME AND POWER SPECTRA

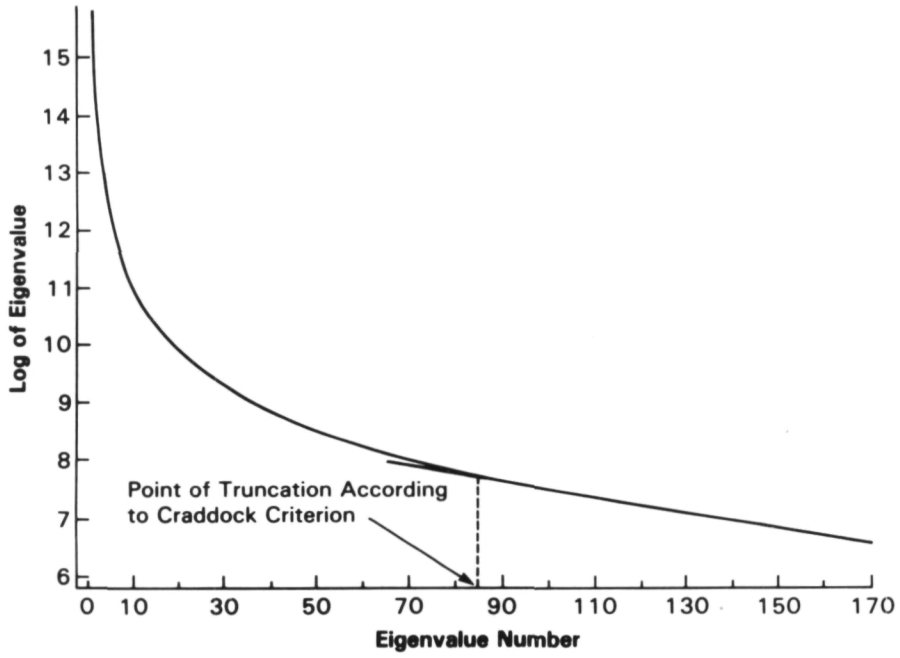

FIGURE 5: LOGARITHM OF EIGENVALUE VERSUS NUMBER

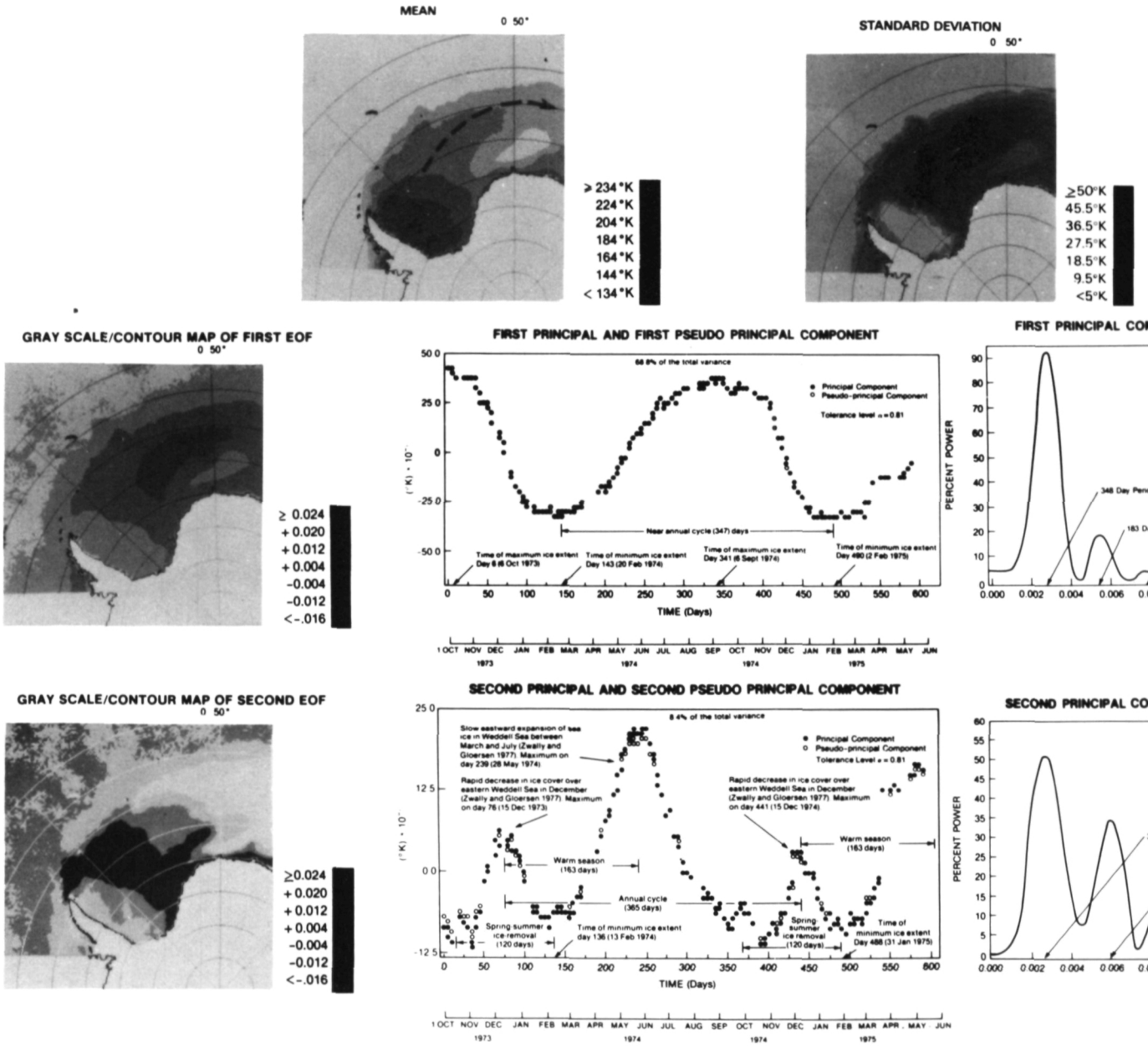

FIGURE 6: MEAN AND STANDARD DEVIATION MAPS, EOF'S 1 AND 2 AND CORRESPONDING PRINCIPAL COMPONENTS AND SPECTRA

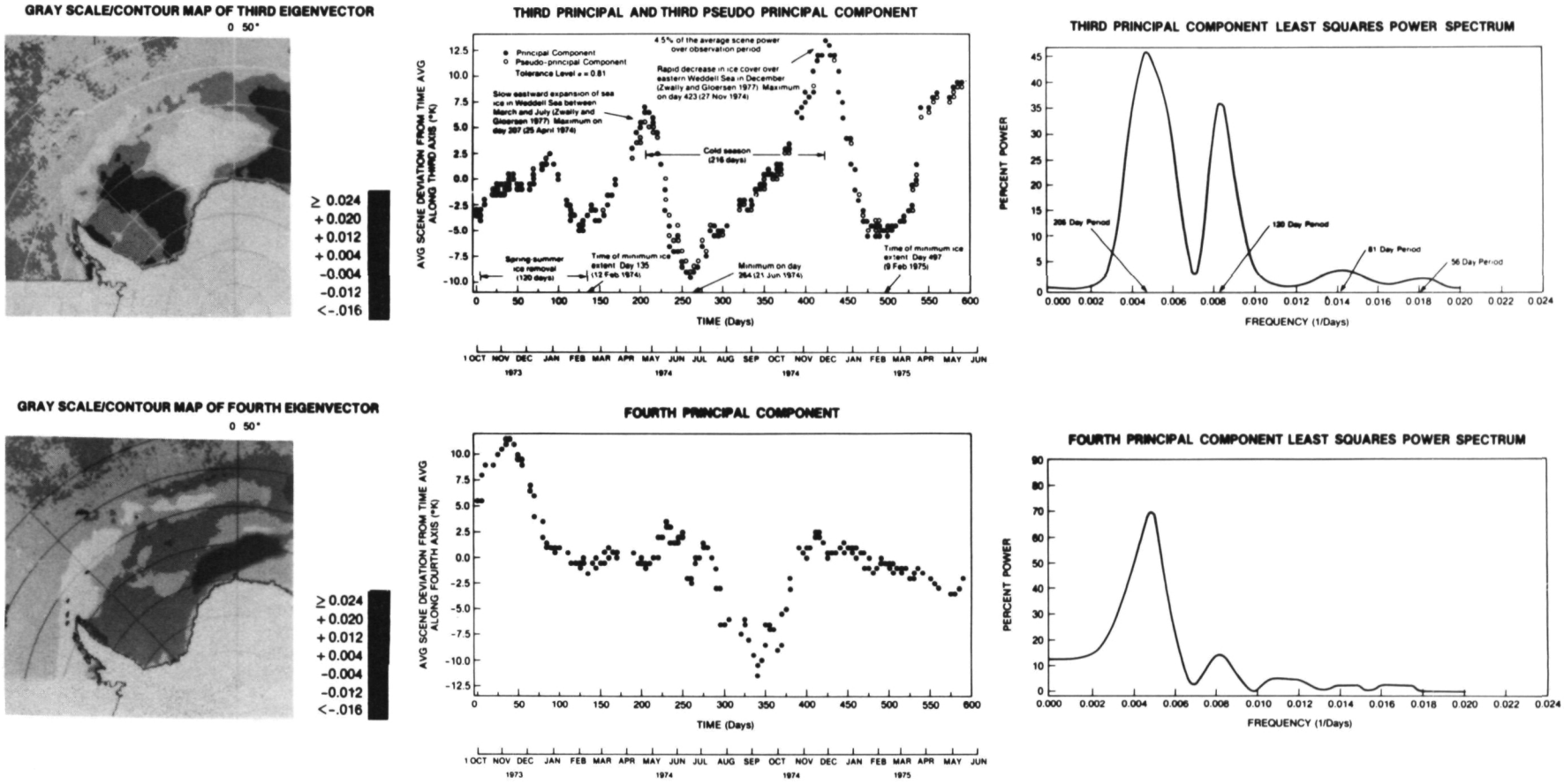

FIGURE 7: EOF'S 3 AND 4, PRINCIPAL COMPONENTS AND SPECTRA

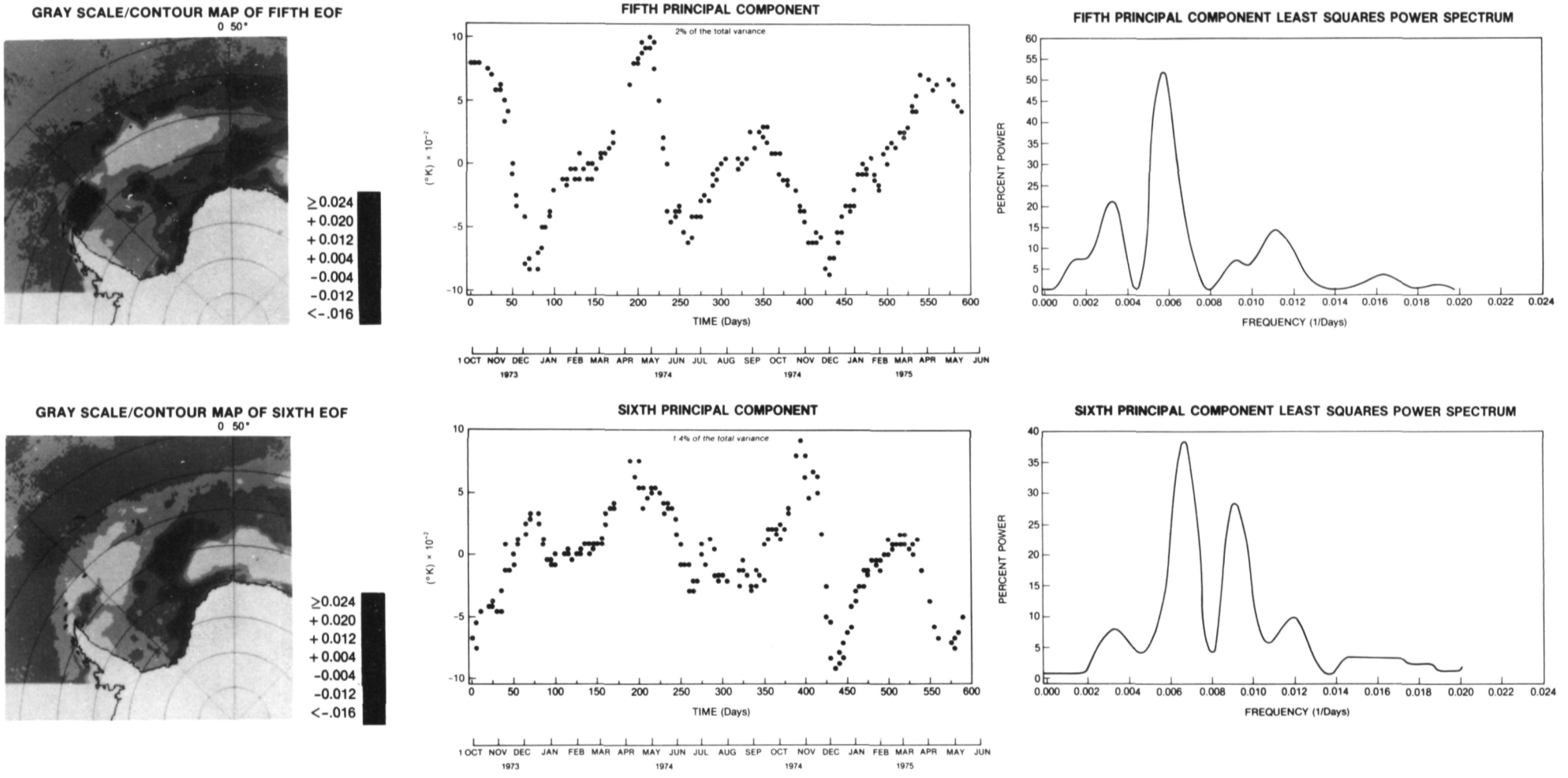

FIGURE 8: EOF'S 5 AND 6, PRINCIPAL COMPONENTS AND SPECTRA

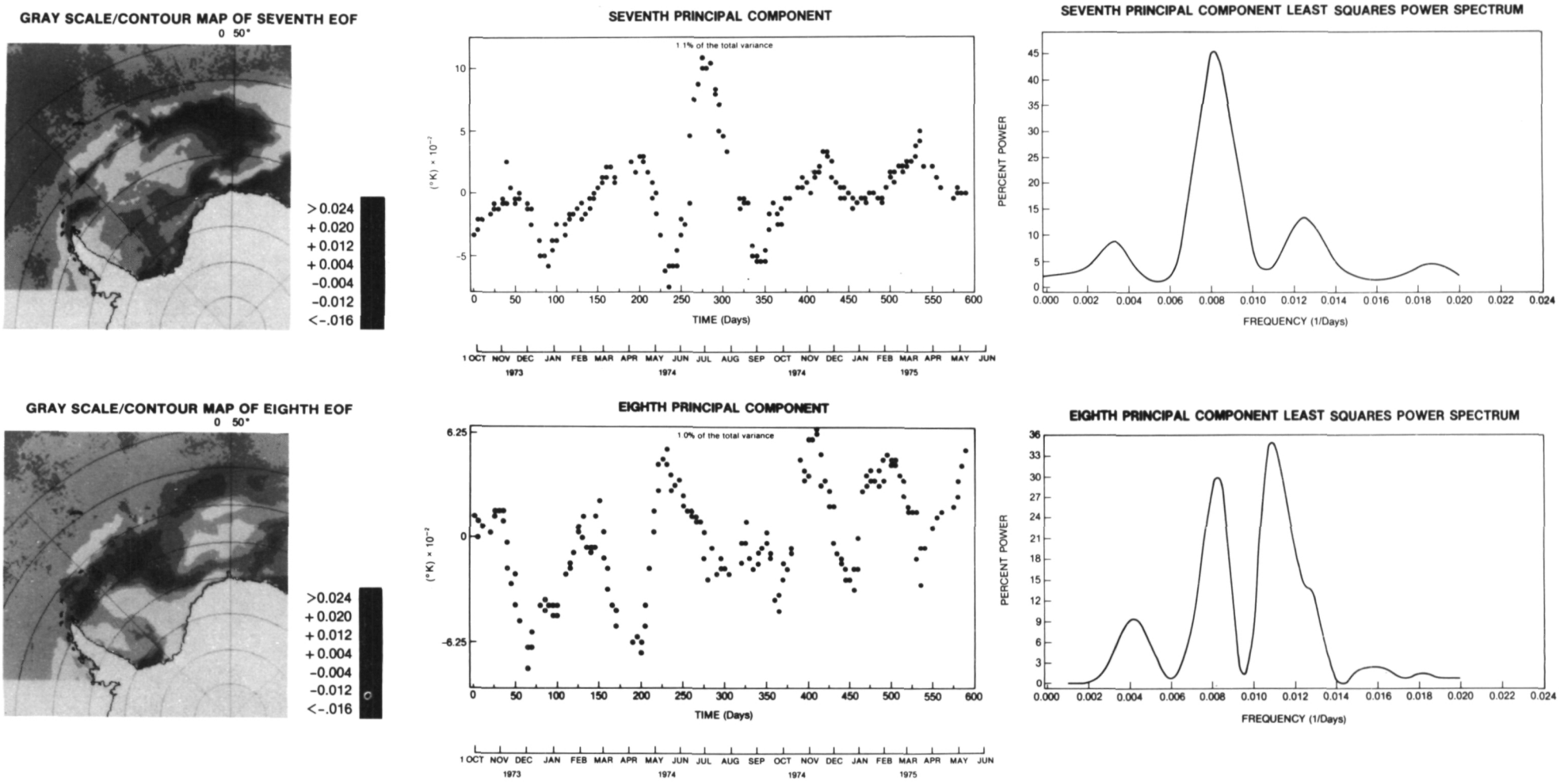

FIGURE 9: EOF'S 7 AND 8, PRINCIPAL COMPONENTS AND SPECTRA

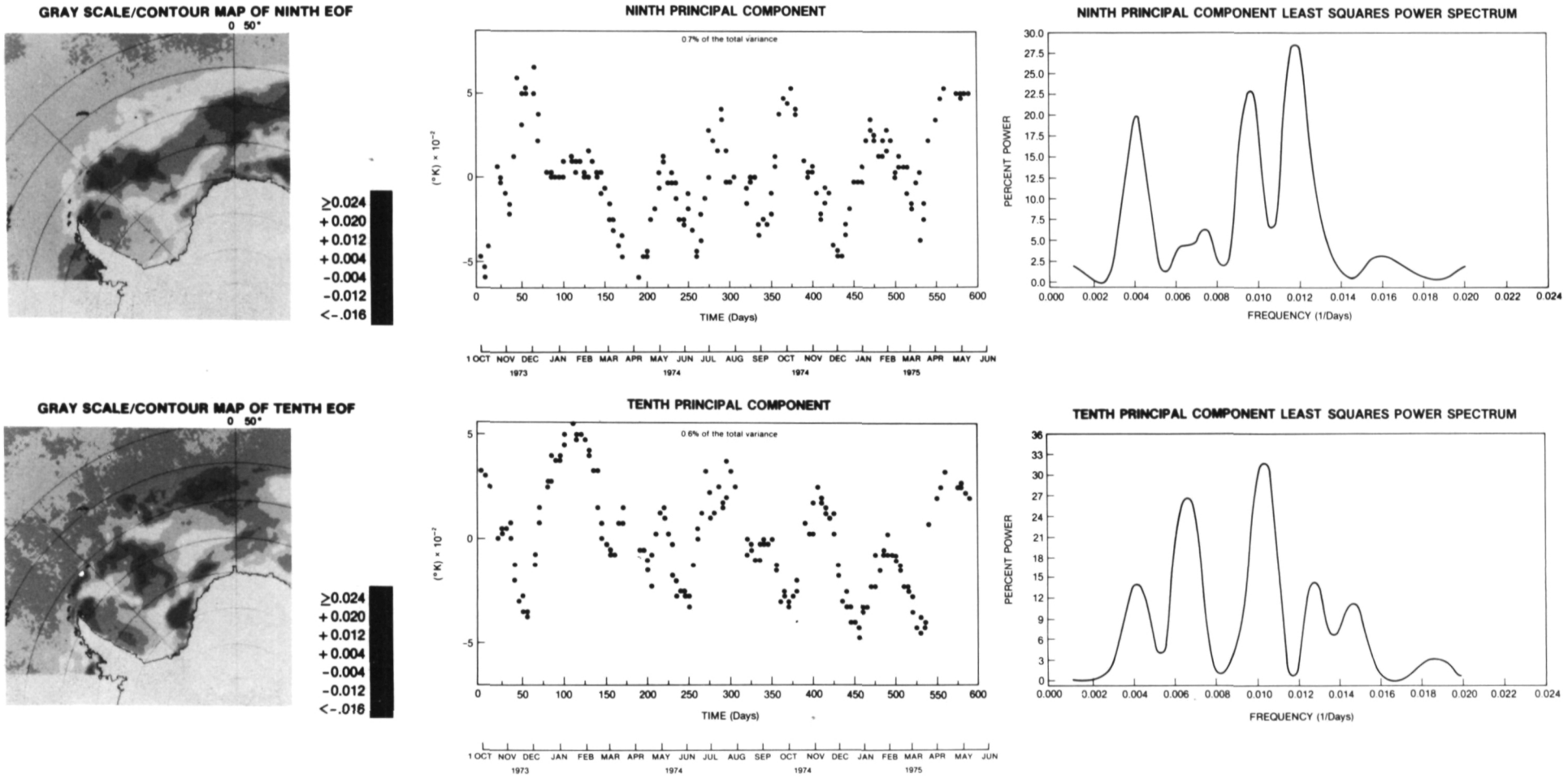

FIGURE 10: EOF'S 9 AND 10, PRINCIPAL COMPONENTS AND SPECTRA

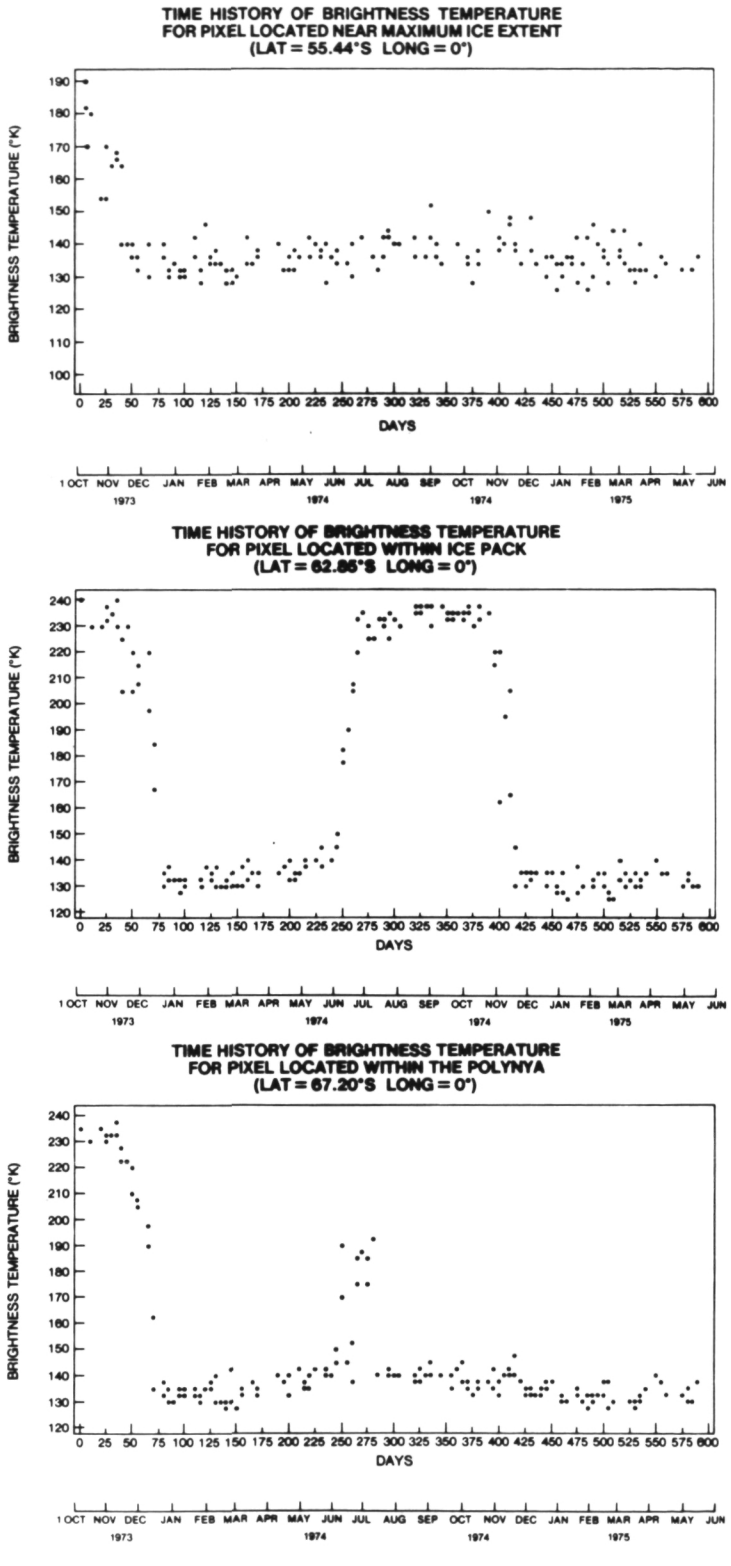

FIGURE 11: TIME HISTORY OF PIXEL BRIGHTNESS TEMPERATURE

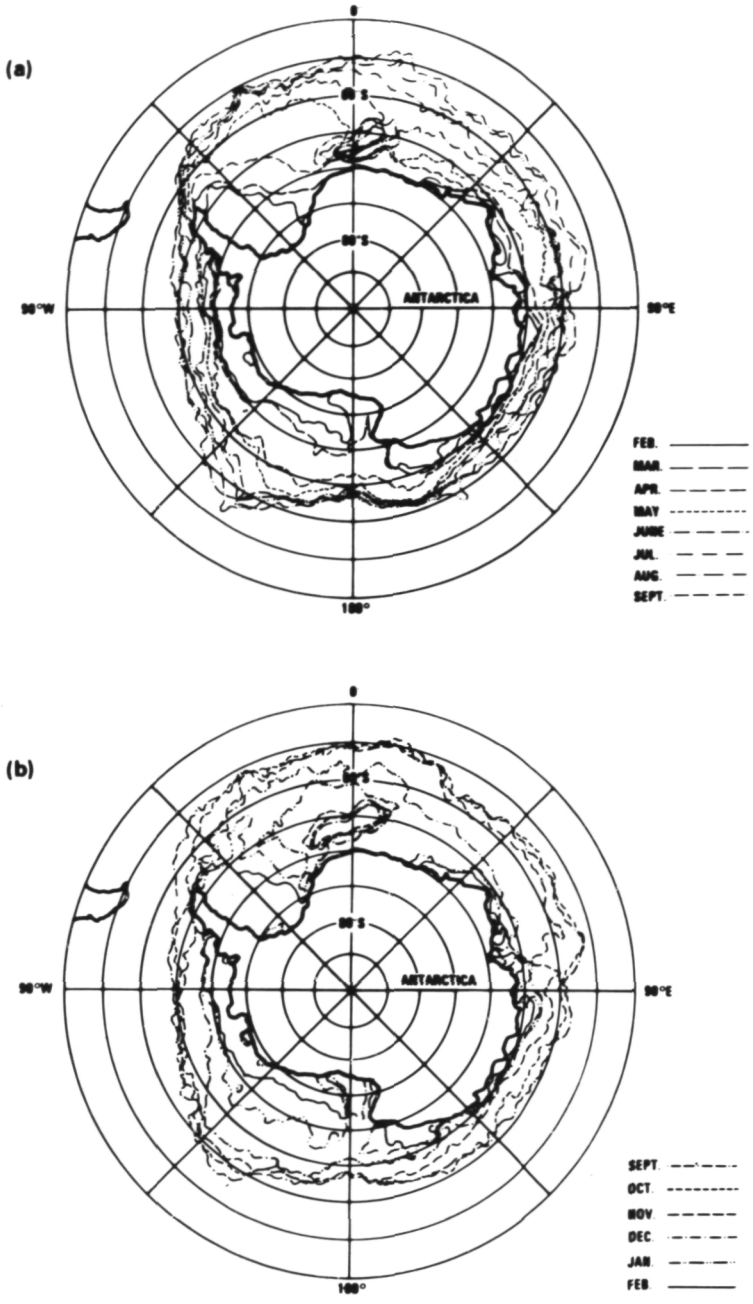

FIGURE 12: MONTHLY AVERAGE SEA ICE EXTENTS DERIVED FROM 1974 ESMR-5 IMAGES: (A) PERIOD OF ICE GROWTH; (B) PERIOD OF ICE DECAY (TAKEN FROM CAVALIERI AND PARKINSON)

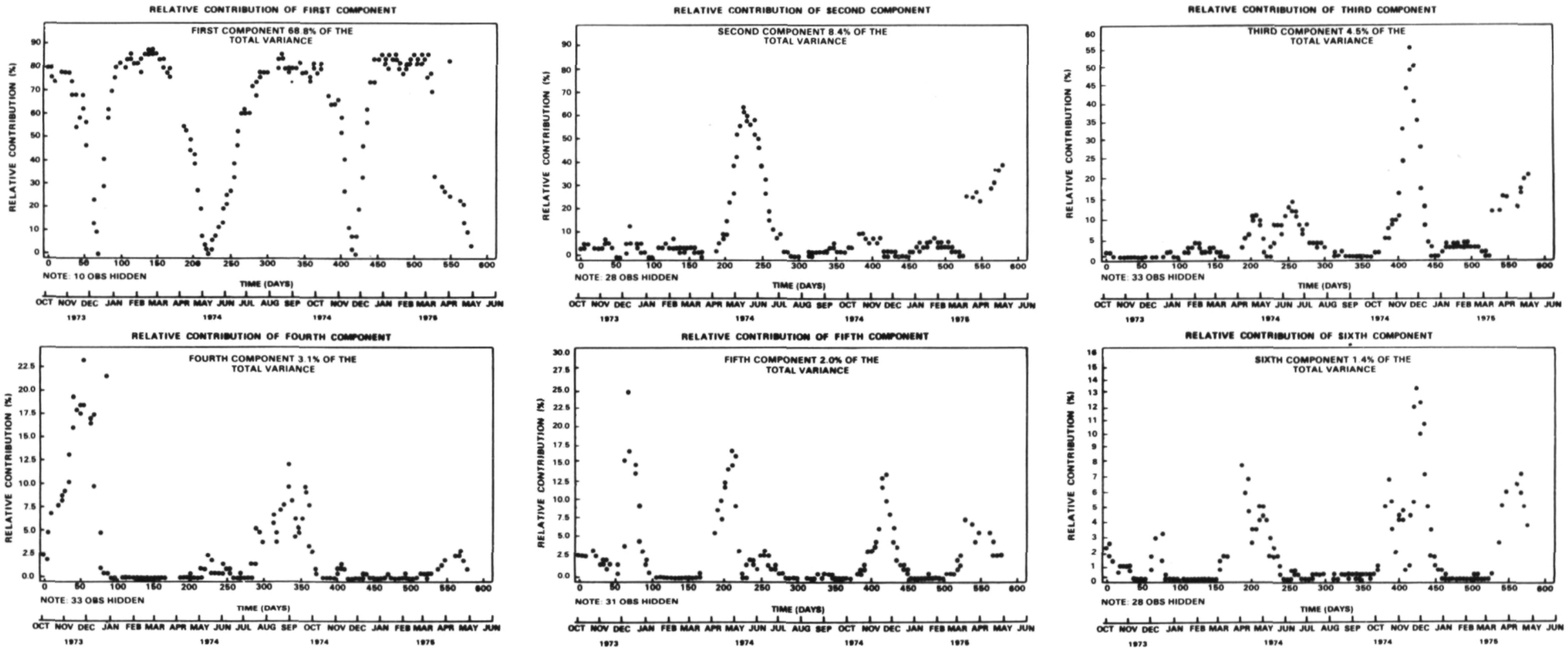

* **Principal component relative contribution** is the percent contribution of the **i**th principal component to the total sum of squares of the **j**th measurement vector v**j** at the **j**th time point.

FIGURE 13: PRINCIPAL COMPONENT RELATIVE CONTRIBUTION*

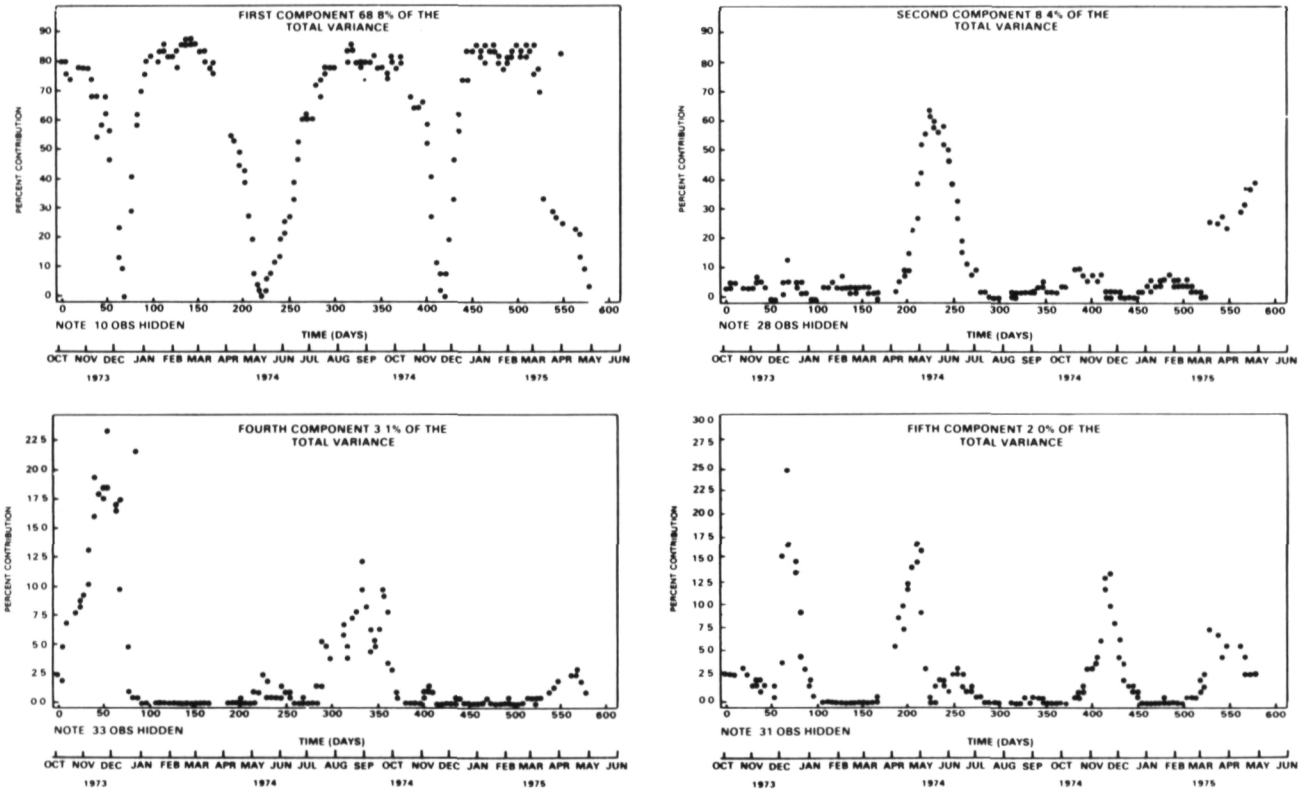

*PRINCIPAL COMPONENT RELATIVE CONTRIBUTION IS THE PERCENT CONTRIBUTION OF THE i^{th} PRINCIPAL COMPONENT TO THE TOTAL SUM OF SQUARES OF THE j^{th} MEASUREMENT VECTOR v_j AT THE j^{th} TIME POINT.

FIGURE 14: PRINCIPAL COMPONENT RELATIVE CONTRIBUTION*